Advanced Drug Sciences

Volume 1 *https://doi.org/xx.xxxx/To Be Assigned* *Issue 1*

Journal Homepage: https://journals2.ums.ac.id/ads/index

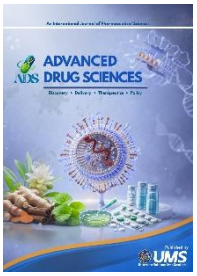

RESEARCH ARTICLE

Design of a Conserved LukS-PV-Based Multi-Epitope Vaccine Candidate Against PVL-Positive *Staphylococcus aureus*: An Immunoinformatics Approach for MRSA and MSSA Coverage

Prottay Choudhury[1], Md. Saiful Islam[1], Synchita Majumder Kaya[1], Umma Salma Mim[1], Shibashish Sarker[1], and K. M. Kaderi Kibria[1]*

[1]Department of Biotechnology and Genetic Engineering, Mawlana Bhashani Science and Technology University, Tangail-1902, Bangladesh.

***Corresponding Author:** Email: km_kibria@yahoo.com; Tel:+88-0921-62407; Fax: +880-921-55400.*

Citation: Choudhury, P., Islam, M. S., Kaya, S., M., Mim, U., S., Ahmed, S., Sarkar, S., Kibria, K. M. K. (2026). Design of a Conserved LukS-PV-Based Multi-Epitope Vaccine Candidate Against PVL-Positive *Staphylococcus aureus*: An Immunoinformatics Approach for MRSA and MSSA Coverage. *Adv. Drug Sci., 1*(1), e000005. DOI: To Be Assigned

Abstract

Background: *Staphylococcus aureus* is a versatile Gram-positive pathogen responsible for a wide range of infections, from mild skin diseases to life-threatening conditions such as pneumonia, sepsis, and endocarditis. Panton–Valentine leukocidin (PVL), particularly its LukS-PV component, is a key virulence factor contributing to immune evasion and tissue damage. As PVL genes occur in both methicillin-sensitive and methicillin-resistant *S. aureus* (MSSA and MRSA), LukS-PV represents a conserved vaccine target. **Objective:** This study aimed to design a conserved LukS-PV-based multi-epitope vaccine candidate against PVL-positive *S. aureus* using an immunoinformatics approach. **Methods:** T-cell and B-cell epitopes from LukS-PV were identified and screened based on antigenicity, conservancy, allergenicity, toxicity, and physicochemical properties. Selected epitopes were evaluated for MHC binding affinity and population coverage. A multi-epitope construct was designed using linkers and an adjuvant, followed by structural modeling, molecular docking with TLR2, molecular dynamics simulation, immune simulation, and in silico cloning. **Results:** The core epitope ITYGRNMDV showed 100% conservancy, while FEITYGRNMDVTHAT showed 95.83% conservancy and strong MHC-II binding with 73.44% population coverage. The vaccine construct demonstrated an antigenicity score of 1.0244 and good solubility. Docking with TLR2 revealed stable binding, supported by molecular dynamics simulation. Immune simulation indicated potential activation of both humoral and cellular responses, and in silico cloning suggested feasible expression in E. coli. **Conclusion:** The designed vaccine construct shows strong in silico potential against PVL-positive *S. aureus*. However, experimental validation is required to confirm immunogenicity, safety, and efficacy.

Article Information

Keywords:
MRSA
Multi-epitope-based vaccine
Population Coverage
Conservancy
LukS-PV

Received	27 May 2026
Revision	28 Jun 2026
Accepted	29 Jun 2026
Published	30 Jun 2026

1. INTRODUCTION

Staphylococcus aureus is a Gram-positive, coagulase-positive pathogen belonging to the *Staphylococcaceae* family [1]. *S. aureus* is an opportunistic pathogen of significant clinical concern due to its capacity to acquire antimicrobial resistance and cause a wide range of infections [2]–[4]. *S. aureus* is a commensal that is frequently present asymptomatically on areas of the human body such as skin, skin glands, and mucous membranes, including the nose and intestines of healthy humans [1]. Studies have revealed that about 20% of individuals are permanent nasal carriers of *S. aureus*, around 30% are intermittent carriers, and approximately 50% are non-carriers [5]. As a result, *S. aureus* is one of the leading causes of the spread of hospital- and community-acquired infections, which have catastrophic repercussions and life-threatening diseases [6]. *S. aureus* causes a wide range of infections, including skin and soft-tissue infections (SSTIs), bone and joint infections, meningitis, osteomyelitis, pneumonia, infective endocarditis, bacteremia, abscesses, and septic shock syndrome [2,7]. High-risk groups for *S. aureus* infection include individuals receiving immunosuppressive or anti-cancer therapy, young children, and low-birth-weight neonates [8] .

Resistance in *S. aureus* emerged rapidly within two years of hospital use of penicillin [6]. MRSA, a major threat to human health, is resistant to antibiotics such as methicillin, penicillin, oxacillin, cloxacillin, cefazolin, and cefoxitin [9]. This resistance is mediated mainly by the acquisition of mecA and, in some strains, mecC, which encode low-affinity penicillin-binding proteins; these resistance determinants are usually carried on the staphylococcal cassette chromosome mec (SCCmec) [10]–[15].

Initially, MRSA was mainly associated with healthcare settings. With time, however, community-associated MRSA (CA-MRSA) emerged and spread among healthy individuals, while hospital-associated MRSA (HA-MRSA) remained a major concern in clinical environments [9]. In addition to antimicrobial resistance, the pathogenic potential of *S. aureus* is strongly influenced by virulence determinants such as Panton–Valentine leukocidin (PVL). PVL is a bicomponent pore-forming leukotoxin encoded by the lukS-PV and lukF-PV genes, which are carried by staphylococcal bacteriophages and can be detected in both methicillin-resistant and methicillin-susceptible *S. aureus* lineages [16,17].

Importantly, PVL is not universally present in all *S. aureus* strains; therefore, PVL-positive *S. aureus* represents a clinically relevant subset rather than the entire MRSA or MSSA population. PVL-positive *S. aureus* has been associated with recurrent skin and soft-tissue infections, tissue necrosis, leukocyte destruction, and severe invasive diseases such as necrotizing pneumonia [17,18]. This distinction is important for the present study because a LukS-PV-targeted vaccine candidate would be most appropriately interpreted as having theoretical relevance against PVL-positive MRSA and MSSA strains, rather than universal coverage against all *S. aureus* isolates. In 2017, the CDC reported that approximately 323,700 people were hospitalized due to MRSA[19]..

In 2019, bacterial antimicrobial resistance was associated with an estimated 4.95 million deaths worldwide, and methicillin-resistant *S. aureus* was the leading pathogen–drug combination, causing more than 100,000 deaths attributable to antimicrobial resistance [20]. In addition to MRSA, methicillin-sensitive *S. aureus* (MSSA) also contributes substantially to the overall burden of *S. aureus* infection [21]. Because PVL genes are present in clinically significant MRSA and MSSA lineages, this study targets conserved Panton-Valentine leukocidin S component (LukS-PV) epitopes to provide theoretical relevance against PVL-positive strains of both types.

Because of antimicrobial resistance, virulence diversity, immune evasion, and the continuing burden of *S. aureus* disease, preventive strategies beyond conventional antibiotics are urgently needed [22]. Epitope-based vaccines offer a promising strategy because they focus on defined antigenic regions recognized by the immune system, thereby enabling a more targeted immune response [23]. Such vaccines can selectively direct immunity against major virulence determinants and may help neutralize bacterial pathogenic mechanisms [24]–[26]. Among PVL-positive *S. aureus* strains, the LukS-PV subunit is especially relevant because it participates in host-cell receptor recognition and promotes assembly of the LukS-PV/LukF-PV toxin complex, ultimately contributing to pore formation, leukocyte damage, and immune evasion [27,28]. The association of PVL-positive *S. aureus* with recurrent skin infections and severe necrotizing pneumonia further supports LukS-PV as a biologically relevant target for epitope-

based vaccine design [29,30]. Despite decades of research, no licensed vaccine against *S. aureus* is currently available [26], mainly due to its genetic variability and complex virulence and immune-evasion mechanisms [31].

The limited success of earlier vaccine strategies highlights the need for conserved, immunogenic targets capable of inducing broad immune responses [32]. An epitope-based approach may also reduce exposure to the full toxin structure by selecting immune-recognition regions rather than the intact LukS-PV protein or complete PVL pore-forming system. Immunoinformatics, genomics, and proteomics now enable systematic prediction of conserved B-cell and T-cell epitopes and the rational design of multi-epitope vaccines [26,33]–[35].

In this study, we used a comprehensive immunoinformatics workflow to design a conserved LukS-PV-derived multi-epitope vaccine candidate targeting PVL-positive *S. aureus*. The workflow included antigen selection, epitope prediction, antigenicity, allergenicity and toxicity screening, conservancy analysis, population coverage estimation, vaccine construction, structural modeling, molecular docking, immune simulation, codon optimization, and in-silico cloning [36,37]. This study aimed to identify a computationally prioritized vaccine candidate with theoretical relevance against PVL-positive *S. aureus*, including PVL-positive MRSA and MSSA strains, for future validation using clinical PVL-positive isolates.

2. MATERIALS AND METHODS

2.1. Vaccine candidate identification

Figure 1 illustrates the overall methodological workflow adopted in this study. At the outset, we performed an extensive literature-based screening to select promising antigenic targets of *S. aureus*. This enabled the rational prioritization of virulence-associated proteins with strong vaccine potential for downstream immunoinformatics analysis. After sorting the proteins, their antigenicity and proper location inside the bacterial cell were assessed. A number of proteins were identified for further analysis (**Table 1)**.

2.2. Assessment of antigenicity and subcellular localization prediction

The National Center for Biotechnology Information (NCBI) database (https://www.ncbi.nlm.nih.gov/) provided the corresponding sequences of the chosen 12 proteins of *S. aureus* [38]. Following that, each protein's FASTA sequence was submitted to the VaxiJen version 2.0 server (https://www.ddg-pharmfac.net/vaxijen/VaxiJen/VaxiJen.html), which assessed each protein's antigenicity using the default parameters [39]. We also validated the antigenicity of the proteins using the Scratch AntigenPro server (https://scratch.proteomics.igb.uci.edu/). LukS-PV was identified as the most antigenic protein in *S. aureus*. Additionally, pSORTb (https://www.psort.org/psortb/) predicted the chosen protein's subcellular location [40].

2.3. Prediction of MHC class I and MHC class II binding

We evaluated the projected affinity of peptides for MHC class I and class II using the IEDB (https://www.iedb.org/) v2.22 (2019-09-04) binding prediction tool and the NetCTL server (https://services.healthtech.dtu.dk/services/NetCTL-1.2/) [41]–[43]. The stabilized matrix base method (SMM) was used to calculate the half-maximal inhibitory concentration (IC50) values of the preselected 9.0-mer epitopes in the setting of MHC class I binding [44].

Every HLA allele was picked for binding prediction, and the length of each allele was set at 9.0 mer. Humans were chosen as MHC donor species because they shared similar alleles. Alleles with IC_{50} values < 250 nM were removed. The preselected 9-mer MHC class I epitopes were considered core peptides and projected into 15-mer epitopes, which were subsequently analyzed using the NetMHCIIpan 4.1 BA method for MHC class II binding analysis. We also extracted MHC class II alleles with IC_{50} values ≤ 250 nM from the IEDB server.

2.4. Population coverage prediction

To assess the efficacy of epitope-based vaccines, we used the IEDB population coverage tools (http://tools.iedb.org/population/) to estimate epitope coverage across high prevalence areas. Given the MHC molecule's vast variability, different races exhibit variable frequencies of HLA expression. This variety is a hurdle since a T-cell epitope that works in one community may not elicit the same response in another [45]. As a result, we computed population coverage for all epitopes using the IEDB population coverage tool and including nation ethnicity as a query. The combined score for MHC class I and II was used to estimate worldwide population coverage, yielding a more nuanced understanding of theoretical vaccine efficacy across diverse global populations.

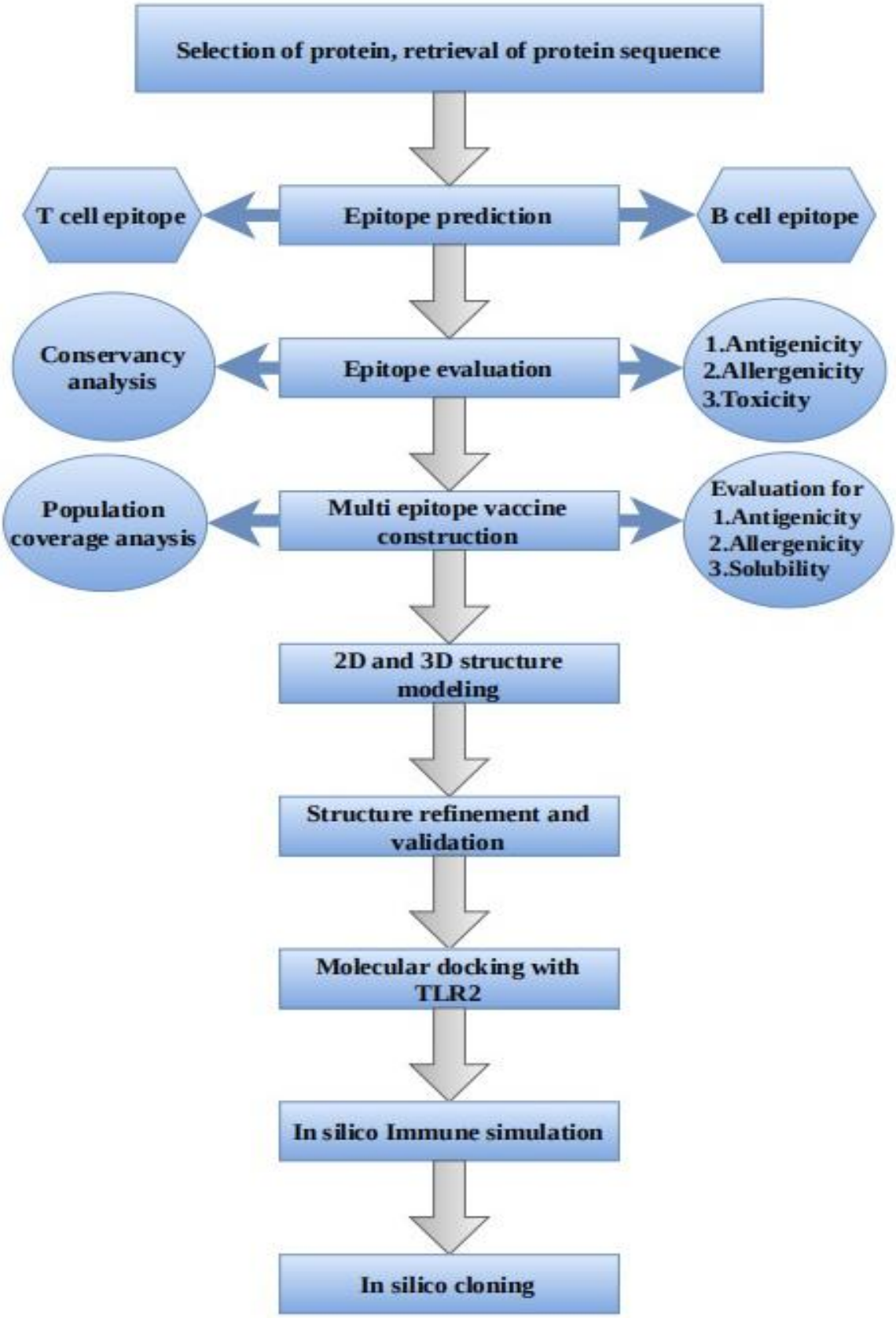

Figure 1. Flow diagram of the entire methodology.

2.5. Conservancy analysis

Compared with conventional MRSA vaccines, the conserved epitope-based vaccine, including Panton-Valentine leukocidin, is projected to provide better protection against PVL-positive MRSA and MSSA strains of *S. aureus*. We collected LukS-PV protein sequences from 824 *S. aureus* strains in FASTA format from the NCBI database for a conservation study. Sequencing errors were decreased, and incomplete sequences were deleted. The IEDB conservancy analysis application (http://tools.iedb.org/conservancy/) was used to thoroughly investigate the conservancy of the projected epitopes [46]. For 9-mer and 15-mer epitopes, the sequence identity threshold value was set at 100%. The conservation level of each potential epitope was evaluated by comparing the 24 LukS-PV protein sequences.

2.6. Allergenicity and toxicity assessment

Investigating a peptide's allergic and toxic properties is critical for preventing adverse effects that could compromise a prospective vaccine candidate. The AllerTOP v2 server (https://www.ddg-pharmfac.net/AllerTOP/) confirmed the allergenicity of the anticipated epitopes by analyzing the data using the Support Vector Machine (SVM) algorithm as well as the sequence composition [47] and later the ToxinPred server was employed (https://webs.iiitd.edu.in/raghava/toxinpred/multi_submit.php) to assess the toxicity using an SVM classifier [48].

2.7. Prediction of the transmembrane helix

TMHMM version 2.0 server (https://services.healthtech.dtu.dk/services/TMHMM-2.0/) was employed to define whether peptides were located in the transmembrane helices of the protein or not [49]. The protein portion falling within the transmembrane region was excluded from the downstream epitope selection criteria.

2.8. Preparation of HLA allele proteins and analysis of their molecular docking interactions

Furthermore, to support the binding prediction between HLA molecules and the recommended epitopes, we ran docking simulations with the best-fit epitope. The crystal structure of the HLA-C*12:03 molecule was selected as a prospective MHC class I candidate, whereas the HLA-DRB1*01:01 molecule was identified as a potential MHC class II candidate. The RCSB protein database (https://www.rcsb.org/) contained the PDB structures **9L47** (Crystal structure of HLA-C*12:03-MY9) and **1T5X** (Crystal structure of HLA-DRB1*01:01 in complex with a synthetic peptide AAYSDQATPLLLSPR and the superantigen SEC3-3B2) [50]. The MHC class I and class II structures were improved by removing the existing ligand from the crystal structure with the BIOVIA Discovery Studio Visualizer (https://discover.3ds.com/discovery-studio-visualizer). Additionally, BIOVIA Discovery Studio Visualizer software was utilized to analyze ligand interactions with receptor amino acids [51].

Table 1. *S. aureus-associated* proteins

Serial No:	Protein Name	Accession Number (No. of aa)	Vaxijen score	Scratch ANTIGENpro	Average Antigenicity	PsortB (score)
1.	LukS-PV	BCD43604.1 (312 aa)	0.7087	0.951152	0.8299	Extracellular (9.98)
2.	PBP2a	ALJ10988.1 (668 aa)	0.6018	0.898597	0.7502	CytM (9.68)
3.	HlgA	AJE65798.1 (321 aa)	o.6432	0.880338	0.7618	Extracellular (9.98)
4.	IsdB	AFH69348.1 (642 aa)	0.7129	0.971910	0.8424	Cell Wall (10.00)
5.	Mntc	AAL50778.1 (312 aa)	0.6437	0.859761	0.7517	CytM (9.68)
6.	Hla	AMQ79365.1 (319 aa)	0.6139	0.946389	0.7801	Extracellular (10.00)
7.	Seb	AAL04126.1 (266 aa)	0.5655	0.854523	0.7100	Extracellular (10.00)
8.	Protein A (SpA)	BAH56724.1 (410 aa)	0.6193	0.882126	0.7507	Cellwall (9.98)
9.	Staphylokinase	EZY46508.1 (163 aa)	0.6388	0.731243	0.6850	Extracellular (10.00)
10.	MR mecR1 protein	CAG9974579.1 (-)	0.5830	0.411167	0.4971	CytM(10.00)
11.	Aureolysin	APE89687.1 (509 aa)	0.6042	0.949943	0.7771	Extracellular (9.98)
12.	LukS-PV	BCD43603.1 (325aa)	0.5638	0.960115	0.7620	Extracellular (9.98)

Aa: Amino Acids; CytM: Cytoplasmic membrane; LukS-PV: Panton-Valentine leukocidin S component; MR: Methicillin resistance

2.9. Prediction of B-cell epitope

Locating and identifying the most immunogenic epitopes within a protein sequence could help reduce the extensive testing required for a prospective vaccine candidate. Presumably, B-cell epitope prediction algorithms can foresee information based on a predicted epitope's humoral immune response [52]. We originally predicted probable B-cell epitopes using the ABCpred server (https://webs.iiitd.edu.in/raghava/abcpred/index.html), which basically examines fixed-length epitopes using an artificial neural network with a scoring threshold of 0.51 [53]. Then we used another B-cell epitope prediction program, Bepipred server (https://services.healthtech.dtu.dk/services/BepiPred-2.0/) [54], successively to screen the best possible B-cell epitopes. Liner epitopes were classified as 0 (0-25%), 1 (26-50%), 2 (51-75%), and 3 (if more than 75% of amino acids were detected) using the screening approach [55].

2.10. Designing a multi-epitope vaccine and assessing its attributes

While designing this vaccine construct, a 50S ribosomal protein L7/L12 adjuvant was placed at the N-terminus to enhance immunogenicity, followed by an EAAAK linker that provides structural rigidity and spatial separation from subsequent domains [56]. Then the construct had its unique 15-mer T-cell and some concentrated B-cell epitopes separated by GPGPG linkers [57], and was finalized with a 6x His-tag for purification at the C-terminal. The T-cell and B-cell epitopes elicit both cellular and humoral immunity, and GPGPG flexible linkers maintain epitope accessibility and reduce junctional immunogenicity [58]. Antigenicity was again screened using Vaxijen, and the AllerTop server was then used to assess the allergenicity of the chimeric vaccine. The solubility of the vaccine for proper expression analysis was assessed using 2 authentic solubility-measuring tools. The first one is the Solpro-scratch tool (https://scratch.proteomics.ics.uci.edu/explanation.html#SOLpro) 59, and the other one is protein-sol (https://protein-sol.manchester.ac.uk/) [59]. The 2D structure of the vaccine was predicted using the PSIPRED Protein Structure Prediction Server (https://bioinf.cs.ucl.ac.uk/psipred/) [60]. 3D structure of the chimeric vaccine was constructed by trRosetta (https://yanglab.qd.sdu.edu.cn/trRosetta/output/TR141574/) [61]. PROCHECK finally assessed the structure's reliability [62].

2.11. Molecular docking of MEV with toll-like receptors

The vaccine must engage with the immune cell receptor in order to initiate an appropriate immunological response. To assess the interaction between the final multi-epitope vaccine and TLR2, we performed docking analysis. The RCSB Protein Data Bank provided the crystal structures of TLR2 (PDB ID 2Z7X). This was performed by using the HDOCK SERVER (http://hdock.phys.hust.edu.cn/) to dock the vaccine's structure with the TLR2 [63]. Another tool, the PDBsum server (http://www.ebi.ac.uk/thornton-srv/databases/pdbsum/Generate.html), was used to identify interacting residues between the Toll-like receptors and the vaccine.

2.12. Molecular Dynamics Simulation

Protein-protein docking was carried out in Schrödinger Maestro (https://www.schrodinger.com/platform/products/maestro/) [64] version 2025.1 (Maestro version 14.3.129; MMshare Version 6.9.129) using the Protein-Protein Docking workflow. In this setup, chain A was treated as the peptide and chain B as the receptor protein. The docking was performed in Standard mode, with 70,000 ligand rotations to probe, a maximum of 5 poses to return, output pose refinement enabled, and preservation of the top 1000 unclustered poses. After docking, the predicted complex was analyzed using the interaction wizard to identify the residues involved at the interface and the types of noncovalent contacts formed between the two chains.

2.13. Immunogenicity evaluation of the vaccine construct

An in silico immune response simulation was conducted using the C-ImmSim (https://kraken.iac.rm.cnr.it/C-IMMSIM/index.php) server to evaluate the immunogenicity of the designed multi-epitope vaccine (MEV) [65]. This platform models the three principal components of the mammalian immune system: bone marrow, thymus, and lymph nodes [65]. The MEV's capacity to elicit responses from various immune cell types—including helper T lymphocytes (HTL), cytotoxic T lymphocytes (CTL), B cells, natural killer (NK) cells, and dendritic cells—as well as the production of immunoglobulins and cytokines, was assessed [66]. Clinically, the minimum recommended interval between two doses of vaccines is four weeks [67]–[70]. Consequently, three injections (each injection contains a thousand units of MEV) were administered using C-ImmSim immunostimulatory, with the recommended interval of

four weeks (1, 84, and 168 time-steps parameters were set as 1 time-step is equal to eight hours of real life) for a total of 1000 steps of simulation. Other parameters were kept at the default.

2.14. *In silico* cloning

Codon adaptation is a way of increasing the translation efficacy of external genes in the host if the use of codons in both species varies. After carefully evaluating MEV properties and immune response, its codon optimization was performed, followed by *in silico* cloning. The Java Codon Adaptation Tool (JCAT) server (https://www.jcat.de/) [71] was used for codon optimization of MEV to make it compatible with the widely used prokaryotic expression system, *E. coli* K12 [72].The GC (guanine and cytosine) contents together with codon adaptation index (CAI) [73] were evaluated. Furthermore, to facilitate restriction and cloning, Eco53KI and BstZ17I restriction enzymes were introduced at the start/N-terminal and end/C-terminal of the optimized MEV sequence, respectively. Finally, the adapted MEV nucleotide sequence was cloned into the E. coli pET28a(+) vector using the SnapGene 4.2 tool (https://snapgene.com/) to ensure *in vitro* expression.

3. RESULTS

3.1. LukS-PV protein of *S. aureus*

A total of 12 *S. aureus* proteins were initially identified through comprehensive literature mining as potential vaccine antigen candidates. The antigenic potential of these proteins was evaluated using VaxiJen v2.0 and ANTIGENpro from the SCRATCH protein prediction suite, which are commonly used for computational prediction of antigenicity and subunit vaccine suitability. Among the screened proteins, LukS-PV ranked as the second most promising antigenic candidate, with an average antigenicity score of 0.8299 (**Table 1**).

Although IsdB showed the highest antigenic score, it was not selected for downstream analysis because the previous IsdB-based V710 vaccine candidate was discontinued due to safety and efficacy concerns, despite IsdB being a conserved, immunogenic, and virulence-associated iron-regulated surface determinant [74,75]. Therefore, LukS-PV was prioritized for further vaccine design. In addition, LukS-PV is a secreted extracellular toxin component of Panton–Valentine leucocidin [76,77]. PSORTb predicted LukS-PV as an extracellular protein with a high localization score of 9.98, supporting its accessibility to the host immune system. The extracellular or secreted nature of LukS-PV strengthens its relevance as a vaccine target, as such proteins are more likely to interact directly with host immune cells and elicit protective immune responses. Finally, through a rigorous selection procedure, the LukS-PV protein sequence of *S. aureus* was extracted from the NCBI database in FASTA format (**Supplementary Table S1**).

3.2. T-Cell epitopes prediction

Using the SMM algorithm, we were able to predict how T-cell epitopes would interact with a variety of MHC class I alleles. Later, the MHC class II interacting epitopes were identified employing IEDB's NetMHCIIpan BA algorithm. The number of HLA-alleles that correspond to each epitope is shown in **Tables 2** and **3**. The 9-mer epitope **ITYGRNMDV** was identified as the core binding region and was further extended into the final 15-mer epitope, FE**ITYGRNMDV**THAT. This extended peptide demonstrated predicted affinity for approximately 206 human HLA alleles, suggesting broad HLA coverage and supporting its selection as a promising candidate for epitope-based vaccine construction.

3.3. Population coverage analysis

The combined population coverage scores for MHC class I and II were determined using IEDB tools to assess their potential as vaccine candidates. The potential epitope "FEITYGRNMDVTHAT" was shown to have **73.44%** population coverage worldwide **(Figure 2** and **Table 4)**. Furthermore, the population coverage data for the epitope was reassessed across regions worldwide. Admittedly, the maximum population coverage of the epitope was observed in West Africa (86.73%), followed by Central Africa (83.19%), North Africa (78.08%), North America (77.88%), East Africa (77.85%), Europe (76.93%), and South Asia (73.01%).

3.4. Prediction of transmembrane helix

The transmembrane helix in the LukS-PV protein sequence was analyzed by TMHMM services. The TMHMM posterior probability plot for the given protein sequence indicated a single transmembrane region located within the first ~30 amino acids, as shown by the purple bars. From **(Figure 3)** we can see that, the protein is predicted to be located outside the membrane (extracellular) for the majority of its length, with high posterior probability (>0.9, orange line). So, while designing the epitopes, we excluded those that fell within the transmembrane region.

Table 2. CD^{8+}T-cell epitopes along with their interacting MHC class I alleles at affinities (IC_{50}) <250 nM.

Epitopes (9-mer)	Interacting MHC class-I alleles (IC50) on the nM scale	No. of alleles
ITYGRNMDV	HLA-C*15:02(25.31), HLA-C*12:03(64.8), HLA-C*16:01(131.9)	3
HATRRTTHY	HLA-C*16:01(28.8), HLA-C*03:02(57.56), HLA-C*12:03(93.84)	3
KAMRWPFQY	HLA-B*58:01(6.25), HLA-A*30:02(9.85), HLA-A*29:02(11.92), HLA-C*16:01(12.45), HLA-A*32:01(16.08), HLA-B*57:01(19.98), HLA-B*15:25(21.54), HLA-C*03:02(22.47), HLA-A*11:01(34.86), HLA-C*12:03(58.87), HLA-A*03:01(133.89)	11
LAATLSLGI	HLA-C*12:03(133.16), HLA-C*16:01(142.31), HLA-C*15:02(146.07)	3
LSLGIITPI	HLA-A*02:06(21.68), HLA-B*58:01(94.13), HLA-A*68:02(101.76), HLA-C*12:03(131.16)	4
MRWPFQYNI	HLA-B*27:05(18.33), HLA-C*06:02(67.54), HLA-C*07:01(123.09), HLA-B*39:01(129.06)	4
RLLAATLSL	HLA-A*32:01(10.04), HLA-A*02:01(11.55), HLA-B*15:25(18.2), HLA-A*02:06(24.82), HLA-B*15:01(88.95), HLA-B*13:01(91.49)	6

Table 3. The potential CD4+ T-cell epitopes, along with their interacting MHC class II alleles, at affinities (IC_{50}) < 250 nM. Alleles with IC50 values less than 50 are shown here, and the rest are shown in **Supplementary Table S3**.

15-mer Epitopes	Interacting MHC class-II alleles (IC50) on the nM scale	Total Alleles
#F**EITYGRNMD**VTHAT	HLA-DRB3*03:01(20.27), HLA-DRB1*13:31(21.81), HLA-DRB1*01:20(36.37), HLA-DRB1*01:10(40.37), HLA-DRB1*15:49(45.72), HLA-DRB1*01:01(46.79), HLA-DRB1*01:05(46.79), HLA-DRB1*01:07(46.79), HLA-DRB1*01:08(46.79), HLA-DRB1*01:12(46.79), HLA-DRB1*01:19(46.79), HLA-DRB1*01:22(46.79), HLA-DRB1*01:25(46.79), HLA-DRB1*01:27(46.79), HLA-DRB1*01:28(46.79), HLA-DRB1*01:30(46.79), HLA-DRB1*01:31(46.79), HLA-DRB1*01:32(46.79), HLA-DRB1*01:18(46.84), HLA-DRB1*14:48(47.72).	206

#Core peptide in bold font

3.5. Analysis of molecular docking

The predicted 9-mer epitope ITYGRNMDV and its 15-mer projection FE**ITYGRNMDV**THAT were found to be properly attached to the HLA-C*12:03 and HLA-DRB1*01:01 grooves independently. The Discovery Studio system visualized the docking simulation and detected and displayed interactions between the 9-mer and 15-mer epitopes, as well as between the HLA-C*12:03 and HLA-DRB1*01:01 amino acid molecules. The CABS-Dock server generated multiple simulations of the docked peptide, and the best was selected for evaluation.

The CABS-dock analysis identified this MHC-I allele-9-mer peptide cluster as the top-ranked representative docking model (**Figure 4**). This cluster exhibited a high density of 84.7741 with 112 elements, indicating strong convergence of peptide conformations toward a similar binding mode. The low average RMSD value of 1.321 Å further suggests that the predicted peptide-binding poses were structurally consistent within the cluster. Although the maximum RMSD was 5.199 Å, the low average RMSD indicates that most conformations remained close to the medoid structure. However, CABS-dock clustering primarily reflects pose convergence and docking stability rather than direct experimental binding affinity.

The docked complex demonstrated multiple stabilizing hydrogen bonds and hydrophobic interactions involving residues CYS164, LYS66, ASN6, and TYR3. However, unfavorable electrostatic interactions between ASP114 and ASP8 suggest localized repulsion within the binding interface. Docking interaction between (FE**ITYGRNMDV**THAT and HLA-DRB1*01:01) has been shown in **Figure 5**, where in both cases, **A.** depicted the cartoon view, and **B.** depicted the surface view. CABS-dock analysis of the 15-mer epitope–MHC class II complex produced a highly populated docking cluster containing 101 elements, with a cluster density of 33.1699. The average RMSD value of 3.04492 Å indicated acceptable convergence of the predicted binding poses around the representative medoid model.

The relatively high maximum RMSD of 14.1682 Å suggests that some conformations displayed greater structural deviation, which may be attributed to the intrinsic flexibility of the extended 15-mer peptide. Since MHC class II molecules accommodate longer peptides

with flexible terminal regions, such variation is not unexpected. Based on the cluster population, density, and average RMSD, the medoid structure was considered the most representative docking model for downstream binding-interface analysis. Entire ligand interactions with the receptor for both cases are shown using Discovery Studio Visualizer in (**Figure 6** and **Figure 7**). Pairs of peptide/receptor residues closer than 4.5 Å in the selected complex (ITYGRNMDV and HLA-C*12:03) are also shown in (**Table 5**), and the ones for (FEITYGRNMDVTHAT and HLA-DRB1*01:01) are displayed in (**Table 6**).

Table 4. Population coverage of the potential peptide in different areas of the world.

Population/Area	Coverage
Central Africa	83.19%
Central America	31.13%
East Africa	77.85%
East Asia	59.99%
Europe	76.93%
North Africa	78.08%
North America	77.88%
Northeast Asia	54.99%
Oceania	45.16%
South Africa	46.75%
South America	53.38%
South Asia	73.01%
Southeast Asia	43.63%
Southwest Asia	62.61%
West Africa	86.73%
West Indies	73.37%
World	73.44%

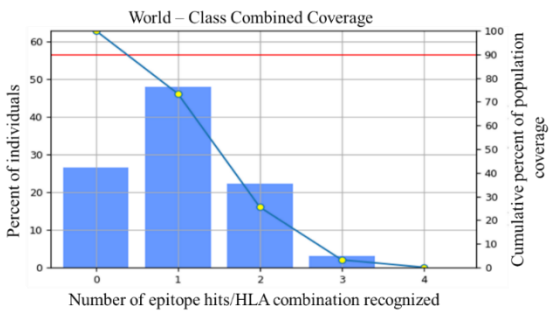

Figure 2. Population coverage - Worldwide Combined Coverage of FEITYGRNMDVTHAT.

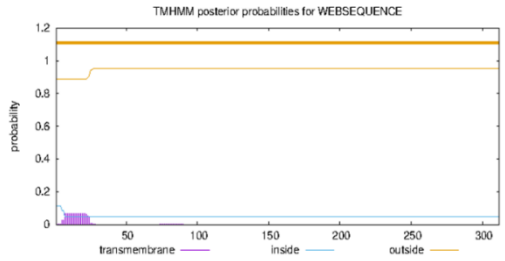

Figure 3. LukS-PV protein's Transmembrane existence evaluation.

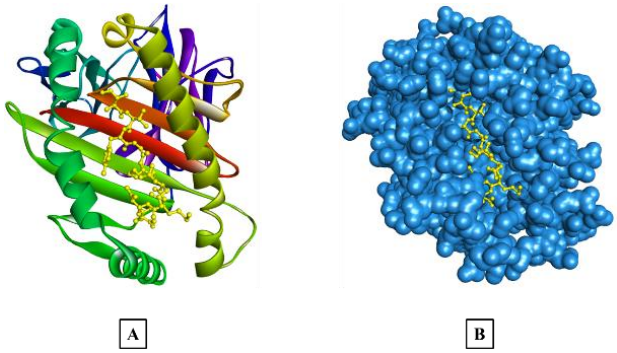

Figure 4. Docking interaction of (ITYGRNMDV and HLA-C*12:03). Here, A: Cartoon view; B: Surface view. (The peptide is shown in yellow in both of the view formats).

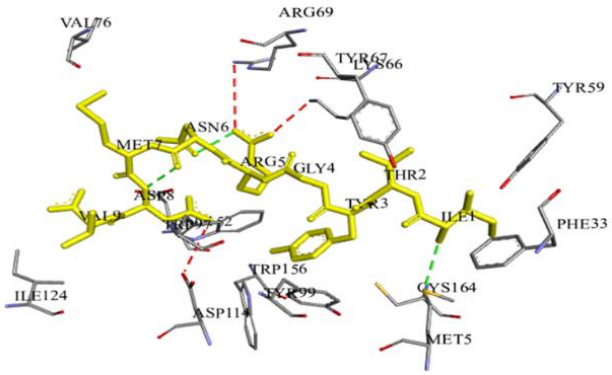

Figure 5. Entire Ligand interaction of ITYGRNMDV (Shown in yellow) and HLA-C*12:03. Green dashes indicate a hydrogen bond, Red dashes indicate an unfavorable interaction, and yellow dashes indicate a hydrophobic interaction.

The latter docked complex exhibited extensive intermolecular interactions involving hydrogen bonds, hydrophobic contacts, and aromatic stabilization. Key peptide residues including TYR2, GLN5, THR7, and SER12 participated in stable receptor interactions with SER53, GLU28, ASN62, and ARG76. However, unfavorable contacts involving ASP4 and TYR78 indicated localized steric or electrostatic strain within the binding interface.

Table 5. Pairs of peptide/receptor residues closer than 4.5 Å in the selected complex (ITYGRNMDV and HLA-C*12:03).

Receptor residue	Peptide residue	Receptor residue	Peptide residue	Receptor residue	Peptide residue
TYR A 159	TYR G 3	TRP A 147	ASP G 8	THR A 143	ASP G 8
GLU A 152	MET G 7	TRP A 133	VAL G 9	ILE A 124	VAL G 9
THR A 143	VAL G 9	TYR A 123	VAL G 9	ASP A 114	ASP G 8
TRP A 133	ASP G 8	TYR A 99	TYR G 3	TRP A 97	ARG G 5
SER A 116	VAL G 9	TRP A 97	GLY G 4	ASN A 80	MET G 7
TRP A 97	ASP G 8	SER A 77	MET G 7	ALA A 73	MET G 7
TRP A 97	TYR G 3	ALA A 73	ASN G 6	GLN A 70	GLY G 4
VAL A 76	MET G 7	GLN A 70	THR G 2	TYR A 67	ILE G 1
GLN A 70	ARG G 5	LYS A 66	ARG G 5	LYS A 66	THR G 2
TYR A 67	THR G 2	GLU A 63	THR G 2	TYR A 59	ILE G 1
LYS A 66	GLY G 4	VAL A 34	ILE G 1	TYR A 7	THR G 2
GLU A 63	ILE G 1	TYR A 7	ILE G 1	GLU A 152	ASP G 8
PHE A 33	ILE G 1	TRP A 167	ILE G 1	GLU A 152	ASN G 6
CYS A 164	TYR G 3	TRP A 156	TYR G 3		

3.6. T-cell and B-cell epitope prediction

First, ABCpred was used to predict the 16-mer B-cell epitope from the LukS-PV amino acid sequence. The top 16-mer epitopes discovered during the analysis are listed in **Supplementary Table S2**. The anticipated B-cell epitopes were then validated by a variety of servers (**Supplementary Table S4**). Using the IEDB conservancy analysis methods, we quantified the conservancy of the top T-cell and B-cell epitopes.

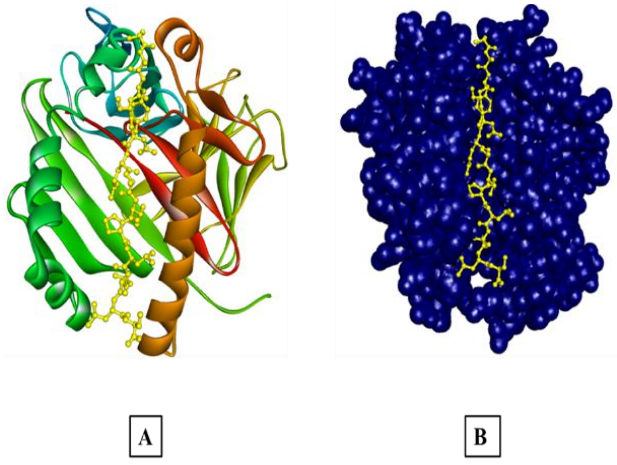

Figure 6. Docking interaction of FEITYGRNMDVTHAT and HLA-DRB1*01:01. Here, A: Cartoon view; B: Surface view. (15-mer peptide is shown in Yellow in both view formats).

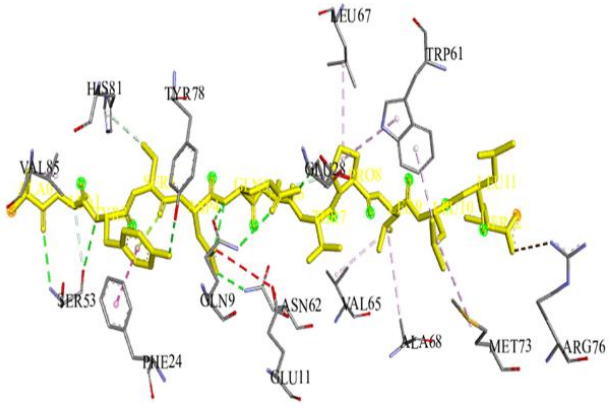

Figure 7. Entire Ligand interaction of FEITYGRNMDVTHAT and HLA-DRB1*01:01. Green dashes indicate hydrogen bonds, Red dashes indicate Unfavorable interactions, Yellow dashes indicate Hydrophobic interactions, Pink/Purple dashes indicate electrostatic interactions.

3.7. Multi-epitope vaccine construction and its sequence analysis

We selected the best T-cell and B-cell epitopes and assessed their conservancy, hydrophobicity, allergenicity, and toxicity using various frequently used techniques (**Table 7**). Some of them exhibited the highest levels of conservation and hydrophilicity in nature. These are also highly immunogenic, non-allergenic, and non-toxic peptides that were selected and joined by the EAAAK-GPGPG linker.

Table 6. Pairs of peptide/receptor residues closer than 4.5 Å in the selected complex (FEITYGRNMDVTHAT and HLA-DRB1*01:01).

Receptor residue	Peptide residue	Receptor residue	Peptide residue	Receptor residue	Peptide residue
TRP D 47	GLU F 2	LYS B 98	THR F 15	MET A 36	ILE F 3
ASP B 152	VAL F 11	TYR A 150	ASP F 10	ASP A 35	ILE F 3
LYS B 98	ALA F 14	THR A 135	ARG F 7	GLU A 30	ARG F 7
TYR A 150	ARG F 7	GLU A 134	ARG F 7	SER A 19	GLU F 2
THR A 135	TYR F 5	SER A 133	MET F 9	GLN A 18	GLU F 2
GLU A 134	TYR F 5	VAL A 132	ASN F 8	TRP D 47	THR F 4
SER A 133	ASN F 8	VAL A 104	ASP F 10	LYS D 46	GLU F 2
VAL A 116	PHE F 1	PRO A 102	HIS F 13	ASP B 152	MET F 9
ASN A 103	THR F 12	GLU A 98	THR F 15	LYS B 98	HIS F 13
GLU A 101	THR F 15	SER A 95	HIS F 13	VAL A 136	TYR F 5
PRO A 96	ALA F 14	LEU A 45	MET F 9	GLU A 134	ASN F 8
ASN A 94	THR F 12	VAL A 42	TYR F 5	SER A 133	ASP F 10
SER A 133	ARG F 7	SER A 133	ARG F 7	HIS A 33	TYR F 5
VAL A 104	THR F 12	VAL A 104	THR F 12	GLY A 20	ILE F 3
PRO A 102	ALA F 14	PRO A 102	ALA F 14	GLN A 18	ILE F 3
GLU A 101	ALA F 14	GLU A 101	ALA F 14	ARG A 44	ARG F 7
SER A 95	ALA F 14	SER A 95	ALA F 14	ALA A 37	ILE F 3
GLU A 46	MET F 9	GLU A 46	MET F 9	ASP A 35	THR F 4
ARG A 44	ARG F 7	ALA A 37	ILE F 3	ASP A 35	THR F 4

Table 7. Examination of the stability of the top epitopes that induce T-cells and B-cells. GRAVY was used to test the hydrophobicity of these peptides. There is more exploration of these peptides' toxicity and allergenicity.

Epitopes	Sequence	Conservancy	Gravy	Allergenicity	Toxicity	Transmembrane region availability	Vaxijen Antigenicity	Vaxijen score
LukS-PV T1	FEITYGRN-MDVTHAT	95.83% (790/824)	-0.453	Non-Allergen	Non-Toxin	No	Antigen	1.4107
LukS-PV B1	SGPSTGG-NGSFNYSKT	83.33% (687/824)	-1.075	Non-Allergen	Non-Toxin	No	Antigen	1.4238
LukS-PV B2	SKSVQW-GIKANSFITS	95.83% (790/824)	-0.138	Non-Allergen	Non-Toxin	No	Antigen	0.6949
LukS-PV B3	SHEKGSGDTS EFEITY	95.83% (790/824)	-1.231	Non-Allergen	Non-Toxin	No	Antigen	2.1377
LukS-PV B4	EVERQNSKSV QWGIKA	95.83% (790/824)	-1.125	Non-Allergen	Non-Toxin	No	Antigen	1.2942
LukS-PV B5	NPSFIAT-VSHEKGSGD	95.83% (790/824)	-0.613	Non-Allergen	Non-Toxin	No	Antigen	1.3447

Table 8. Vaccine construction using different linkers and evaluation of solubility.

Vaccine Design	Adjuvants	Linker	VS	VA	Allertop	SSP	PS
MADLK-NFAEQLVNLTVKEVNELAQILKDEYGIEPAAAA-VAVAGVAGGGADAA-TAEEKTEFTVVLKSAGASKLAVVKLVKELTGQGL KEAKELVDGAPSTLKEGVSKDEAEGLKKALEEA-GAEVELKEAAAKFEITYGRN-MDVTHATGPGPGSGPSTGGNGSFNYSKTGPGPG SKSVQWGIKANSFITSGPGPGSHEKGSGDTSE-FEITYGPGPGEVERQNSKSVQWGIKAG-PGPGNPSFIATVSHEKGSGDHHHHHH	MADLK-NFAEQLVNLTVKEVNELAQILKDEYGIE PAAAAVAVAGVAGGGADAA-TAEEKTEFTVVLKSAGASKLAV-VKLVKELTGQGLKEAKEL-VDGAPSTLKEGVSKDEAEGLKKALEEA GAEVELK	EAAAKand GPGPG	1.0244	Ag	NON-Allergen	0.988235	0.837

Ag: Antigen; VA: Vaxigen antigenicity; VS: Vaxigen Score; SSP: Solpro-scratch (probability); PS: Protein-sol

An adjuvant named 50S ribosomal protein L7/L12 was added to the N-terminal of the multi-epitope vaccine, which can be used to enhance the immunogenicity and finalized with a 6x His-tag in the later portion for purification purposes **(Figure 8).** The resulting multi-epitope vaccination was 257 amino acids long (26.31kDa) with an isoelectric pH of 5.52. The solubility of the vaccine for proper expression analysis was conducted with 2 tools: Protein-sol, where the value of 0.837 (greater than 0.5) signifies good solubility, and the Solpro-scratch tool, in which a value of 0.988235 closer to 1 validates the proper solubility of the vaccine **(Table 8)**. The vaccine has a negative GRAVY value (-0.467), indicating it is hydrophilic **(Table 7)**.

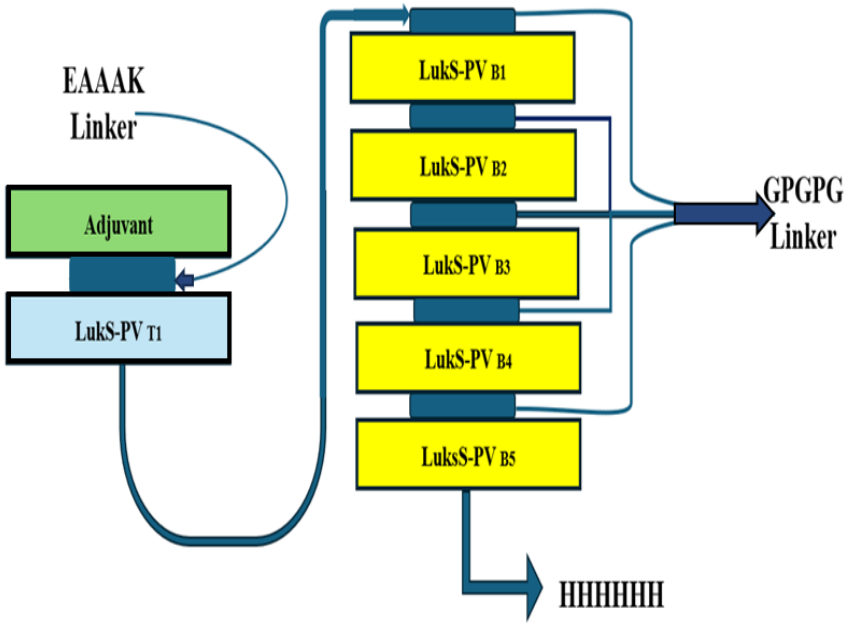

Figure 8. Schematic diagram of the final multi-epitope.

After analyzing the physical parameters, the secondary structure was predicted using PSIPRED (Fig. 9A), and the three-dimensional structure was constructed using trRosetta (**Figure 9**). The secondary structure analysis was performed to determine the distribution of major structural elements within the protein sequence. The prediction indicated the presence of ordered secondary-structure regions alongside flexible coil segments, suggesting that the construct possesses both structured domains and accessible regions that may contribute to epitope exposure. The predicted secondary structural pattern was further used to support tertiary structure modeling.

The three-dimensional structure generated using trRosetta showed a TM-score of 0.520, indicating an acceptable overall fold prediction with moderate structural reliability. Since TM-scores above 0.5 generally suggest a meaningful global topology rather than a random fold, the modeled structure was considered suitable for downstream refinement, validation, and molecular docking analysis. The final 3D structure of MEV was validated using Ramachandran plot analysis in PROCHECK. The PROCHECK server indicates that 94.1% of residues in the predicted model are in the most favored regions, 5.4% are in additional allowed regions, and 0% are in disallowed regions in the Ramachandran plot (**Figure 9C**).

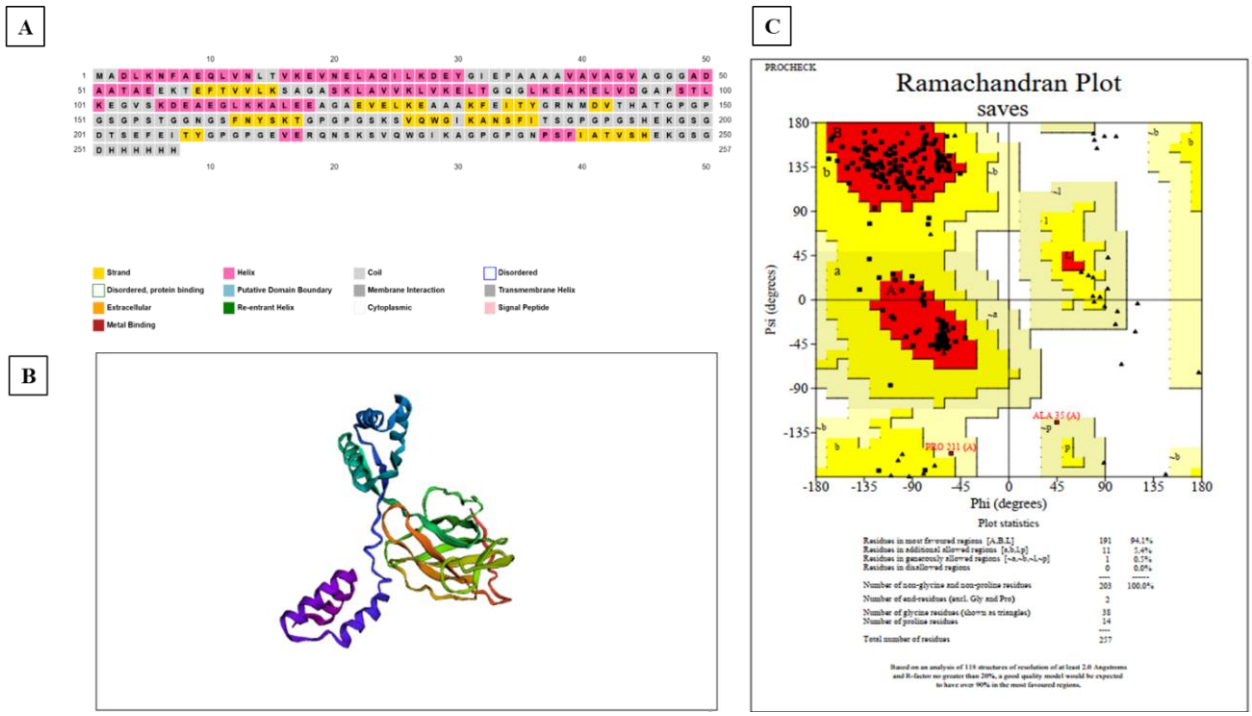

Figure 9. A: The 2D structure generated by the PSI-PRED server; B: 3D model of the multi-epitope vaccine construct modeled by trRosetta; C: Ramachandran plot analysis utilizing the PROCHECK server for the corresponding 3D model.

3.8. Molecular docking of MEV with toll-like receptor

The resulting multi-epitope vaccination was docked with a Toll-like receptor to determine its ability to elicit an innate immune response. The docking analyses were performed using the HDOCK online server, indicating that naturally occurring interactions between our proposed MEV and TLR2 may be energetically favorable. (**Figure 10A**) depicts the docking relationship between MEV and TLR2.Consequently. PDBsum analysis of the docked complex revealed a stable interaction interface between Chain A and Chain B, involving 5 salt bridges, 11 hydrogen bonds, and 164 non-bonded contacts (**Figure 10C** and **D**).

The salt-bridge network was mainly formed by Lys79(A)-Asp334(B), Glu122(A)-His78(B), Glu117(A)-His116(B), Glu124(A)-Lys33(B), and Lys126(A)-Asp30(B). In addition, hydrogen-bonding interactions were observed between residues including Lys79(A)-ASP354(B), Ala69(A)-Ser219(B), Ala69(A)-His193(B), Ser70(A)-Glu217(B), Glu118(A)-Lys166(B), Ala119(A)-Lys166(B), Glu88(A)-Glu407(B), Glu88(A)-GLU380(B), Glu117(A)-Tyr97(B), Glu124(A)-Lys33(B), and Glu124(A)-Ser32(B). The presence of multiple electrostatic interactions, hydrogen bonds, and extensive non-bonded contacts suggests favorable interface stabilization between the interacting chains.

3.9. Molecular Dynamics Simulation

The predicted protein-protein docking complex between the vaccine construct and TLR2, generated using the Protein-Protein Docking module of Schrödinger Maestro, is shown in **Figure 11**. The docking produced a single dominant binding pose in which chain A occupied a surface region of chain B and formed contacts mainly with residues B:ILE37, B:HIS38, B:VAL39, B:PRO40, B:LYS41, and B:ASP42 on the receptor side, and A:LYS79, A:GLU80, A:LEU81, A:THR82, A:GLY83, A:GLN84, A:GLY85, A:LEU86, and

A:LYS101 on the peptide side. The interaction profile showed that the interface was primarily driven by close van der Waals contacts; however, several of these interactions were associated with steric clashes, particularly around A:LYS79, A:THR82, and A:LYS101, indicating local steric strain within the docked conformation.

A total of two hydrogen bonds were identified: one between B:ILE37 and A:LEU81 (1.5 Å), and another between B:GLY35 and A:LYS101 (1.1 Å), although the latter was accompanied by a steric clash with A:LYS101, suggesting unstable local geometry at that region. In addition, a salt bridge was observed between B:ARG31 and A:GLU80 (1.0 Å), indicating a potential electrostatic contribution to interface stabilization. No π-stacking or disulfide interactions were detected in the docked complex (**Table 9**).

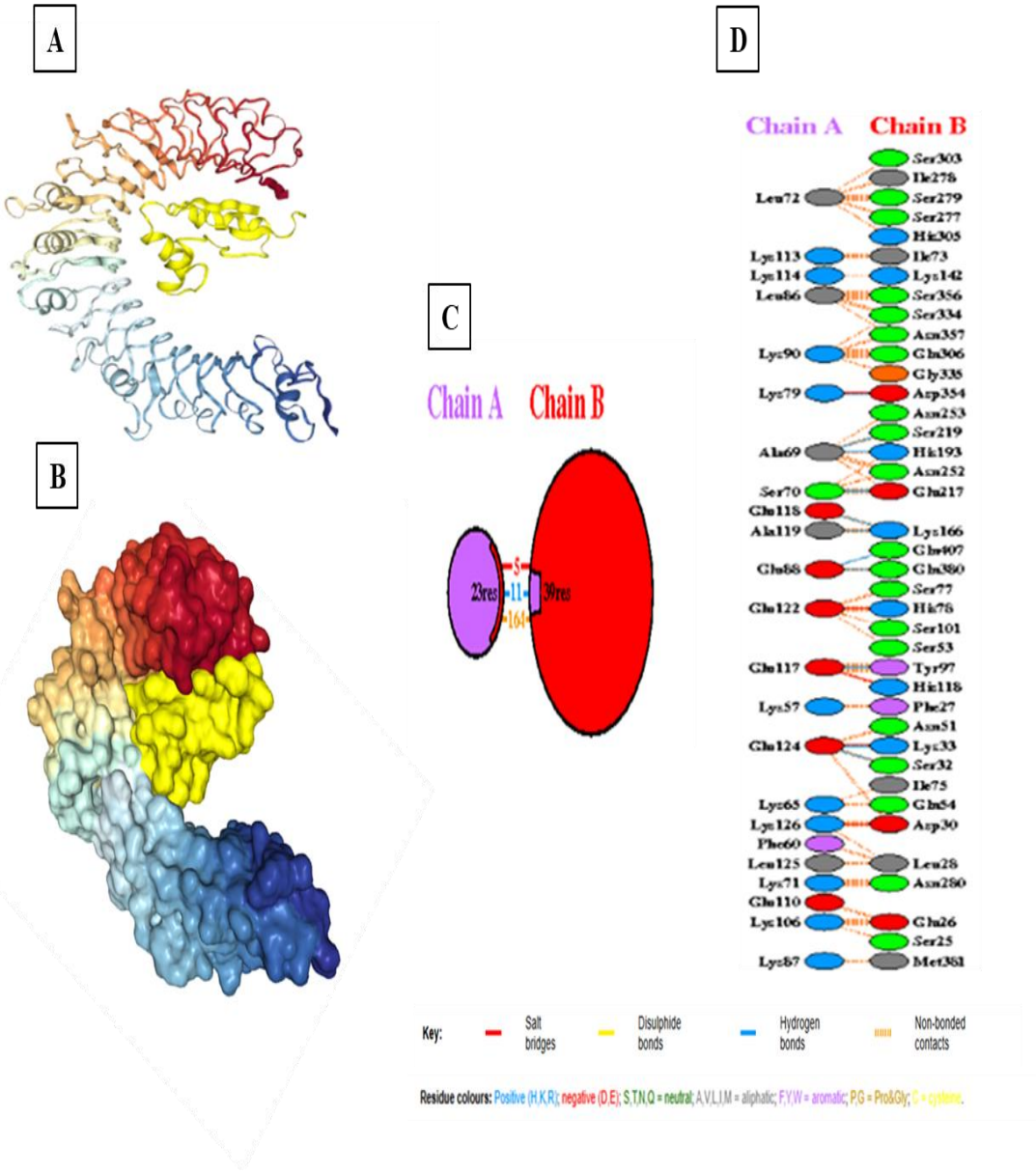

Figure 10. Docking of MEV with the Toll-like receptors. A: Cartoon representation of the docked complex with TLR2; B: Surface representation of the docked complex with TLR2; C: Protein-protein chain interface; D: Different interacting residues extracted by the PDBsum server.

The surface complementarity and buried SASA values confirm the formation of a defined protein-protein interface; however, the presence of multiple short-distance clashes alongside limited stabilizing interactions suggests that the predicted binding pose may represent a close-contact docking solution rather than a fully relaxed and energetically stable complex. Therefore, further structural refinement through energy minimization and molecular dynamics simulations is required to assess the persistence and stability of the observed hydrogen-bonding and salt-bridge interactions under dynamic physiological conditions.

Table 9. Inter-residue interaction profile of the peptide–peptide docked complex after molecular dynamics simulation.

Set1 Residues	Set2 Residues	Distance (Å)	Specific Interactions	H-Bond	H-Bond % Poses	Salt Bridges	Salt Bridges % Poses	Pi Stacking	Pi Stacking % Poses
B:TYR 56	A:LYS 101	1.8 Å	1x clash to A:LYS 101	0	0	0	0	0	0
B:TYR 56	A:GLU 108	2.3 Å	1x clash to A:GLU 108	0	0	0	0	0	0
B:ASP 42	A:LYS 79	1.2 Å	5x clash to A:LYS 79	0	0	0	0	0	0
B:HIS 38	A:THR 82	1.2 Å	3x clash to A:THR 82	0	0	0	0	0	0
B:HIS 38	A:GLY 83	1.3 Å	2x clash to A:GLY 83	0	0	0	0	0	0
B:ILE 37	A:LYS 101	0.8 Å	11x clash to A:LYS 101	0	0	0	0	0	0
B:ILE 37	A:LEU 81	1.5Å	1x hb to A:LEU 81	1	1	0	0	0	0
B:ILE 37	A:THR 82	1.2 Å	1x clash to A:THR 82	0	0	0	0	0	0
B:LEU 36	A:LEU 81	0.7Å	11x clash to A:LEU 81	0	0	0	0	0	0
B:GLY 35	A:LYS 101	1.1 Å	1x hb, 1x clash to A:LYS 101	1	1	0	0	0	0
B:ASN 34	A:LEU 81	0.9 Å	4x clash to A:LEU 81	0	0	0	0	0	0
B:ARG 31	A:GLU 80	1.0Å	1x salt bridge to A:GLU 80	0	0	1	100	0	0

3.10. Immunogenicity evaluation of the vaccine construct

The immune simulation of the MEV provides a comprehensive overview of both humoral and cellular immune responses following antigen exposure. The simulation results in (**Figure 12**), (i) demonstrate rapid antigen clearance accompanied by a robust antibody response, characterized by an early peak in IgM levels followed by sustained IgG production. (ii) reveals dynamic changes in B cell populations, with a significant increase in memory B cells and a class switch from IgM to IgG isotypes, indicative of the development of long-lasting immunity. (iii-iv) illustrate the activation, proliferation, and memory formation of helper T cells, while **(v)** shows similar patterns in cytotoxic T cells, with both cell types transitioning from active and proliferative states to stable memory pools. (vi) highlights the temporal regulation of cytokine secretion, with early peaks of IFN-γ and IL-2 driving the initial immune activation. Finally, Panels (vii-viii) emphasize the critical roles of natural killer (NK) cells and dendritic cells in the early innate response and sustained adaptive immunity, respectively. Collectively, these simulation results depict a tightly coordinated interplay between innate and adaptive immune components, supporting effective pathogen clearance and the establishment of durable MEV-induced immunological memory.

Figure 11. Predicted protein–protein docking complex between chain A (peptide, cyan) and chain B (protein, green) generated using the Protein–Protein Docking module of Schrödinger Maestro.

3.11. *In silico* Cloning

In silico cloning was performed to ensure expression of SARS-CoV-2-derived MEV in a commonly used *E. coli* host. First, the codons of the MEV construct were adapted as per the codon usage of the *E. coli* expression system. The JCAT server was used to optimize the MEV codons for *E. coli* (strain K12). The optimized MEV construct contained 771 nucleotides, an ideal range of GC content 50.45% (30–70%), and a CAI

value of 0.925 (0.8–1.0), and showed a high possibility of positive protein expression and reliability. In the next step, Eco53KI and BstZ17I restriction sites were added to both ends of the MEV-optimized nucleotide sequence to facilitate cloning. Finally, the refined MEV sequence was cloned between Eco53KI and BstZ17I restriction sites at the multiple cloning site of the pET28a (+) vector (**Figure 13**). The total length of the clone was 3.327 kbp.

4. DISCUSSION

As LukS-PV is a virulence-associated toxin component rather than a methicillin-resistance determinant, the proposed vaccine target should be interpreted in the context of PVL-positive *S. aureus*. PVL genes can be present in both MRSA and MSSA strains and are commonly associated with phage-mediated transfer across diverse *S. aureus* lineages [78,79]. Therefore, the conserved LukS-PV-derived epitopes identified in this study may provide theoretical coverage against PVL-positive MRSA and MSSA strains, rather than universal protection against all MRSA and MSSA isolates. MRSA pathogenesis begins with colonization of the skin or mucous membranes, where bacterial adhesion is mediated by surface proteins such as clumping factors and fibronectin-binding proteins [80]. Tissue invasion may then be promoted by enzymes such as lipases and hyaluronidase, which degrade extracellular matrix components [81].

In many severe community-associated *S. aureus* infections, PVL acts as an important virulence factor. It is a bicomponent pore-forming toxin composed of LukS-PV and LukF-PV, which targets human leukocytes and contributes to immune evasion and tissue injury [27,82]. PVL-mediated cytotoxicity depends on receptor engagement, interaction between the S and F components, oligomerization, and pore formation in host immune-cell membranes [30,83].

This mechanism is important for the safety interpretation of the present design because the proposed construct contains selected epitopes rather than the intact LukS-PV/LukF-PV toxin system. Therefore, it is not expected to retain the complete structural machinery required for PVL-like pore formation, although this remains a computational inference requiring experimental validation.

The complexity of *S. aureus* immunity and the repeated failure of previous vaccine candidates highlight the need for more rational antigen-selection strategies [84]. Immunoinformatics can support early vaccine design by enabling rapid screening of antigenicity, epitope conservation, allergenicity, toxicity, HLA binding, structural stability, and immune simulation before laboratory validation [85]. In the present study, candidate antigenic proteins were selected through literature mining and evaluated using VaxiJen, ANTIGENpro, and PSORTb. Among the screened proteins, LukS-PV emerged as a highly antigenic extracellular (secreted) candidate **(Table 1)**. Although IsdB showed the highest predicted antigenicity score, it was excluded because of the limitations discussed earlier. Thus, LukS-PV was prioritized based on its predicted antigenicity, extracellular/secreted localization, relevance to virulence, and accessibility to the host immune system.

The LukS-PV protein sequence was retrieved from NCBI using accession ID BCD43604.1 **(Table S1)**. Initial T-cell epitope prediction identified KAMRWPFQY, RLLAATLSL, MRWPFQYNI, LSLGIITPI, ITYGRNMDV, LAATLSLGI, and HATRRTTHY as peptides with strong predicted binding affinity for MHC class I alleles. Further analysis identified **ITYGRNMDV** as the core 9-mer epitope, which was extended to the 15-mer peptide FE**ITYGRNMDV**THAT for MHC class II prediction. Conservancy is critical for vaccine-candidate selection because conserved epitopes may support broader strain coverage and reduce immune escape [86]. In the analyzed *S. aureus* sequences, ITYGRNMDV and FEITYGRNMDVTHAT showed high conservancy, with 100.00% and 95.83% conservation, respectively, supporting their theoretical relevance for PVL-positive *S. aureus* strains. The 15-mer peptide FEITYGRNMDVTHAT also showed an estimated global population coverage of 73.44% (**Table 4**), indicating broad predicted HLA coverage.

However, this value represents theoretical population coverage and should not be interpreted as direct evidence of protective efficacy. Peptide-based vaccines offer advantages over full-protein vaccines, including easier synthesis, improved chemical stability, reduced unnecessary antigenic load, and focused immune targeting [87]. Surface accessibility is also important because accessible antigenic regions are more likely to be recognized by antibodies or antigen-presenting cells. The selected peptide was predicted to be located in an accessible region of the modeled LukS-PV structure.

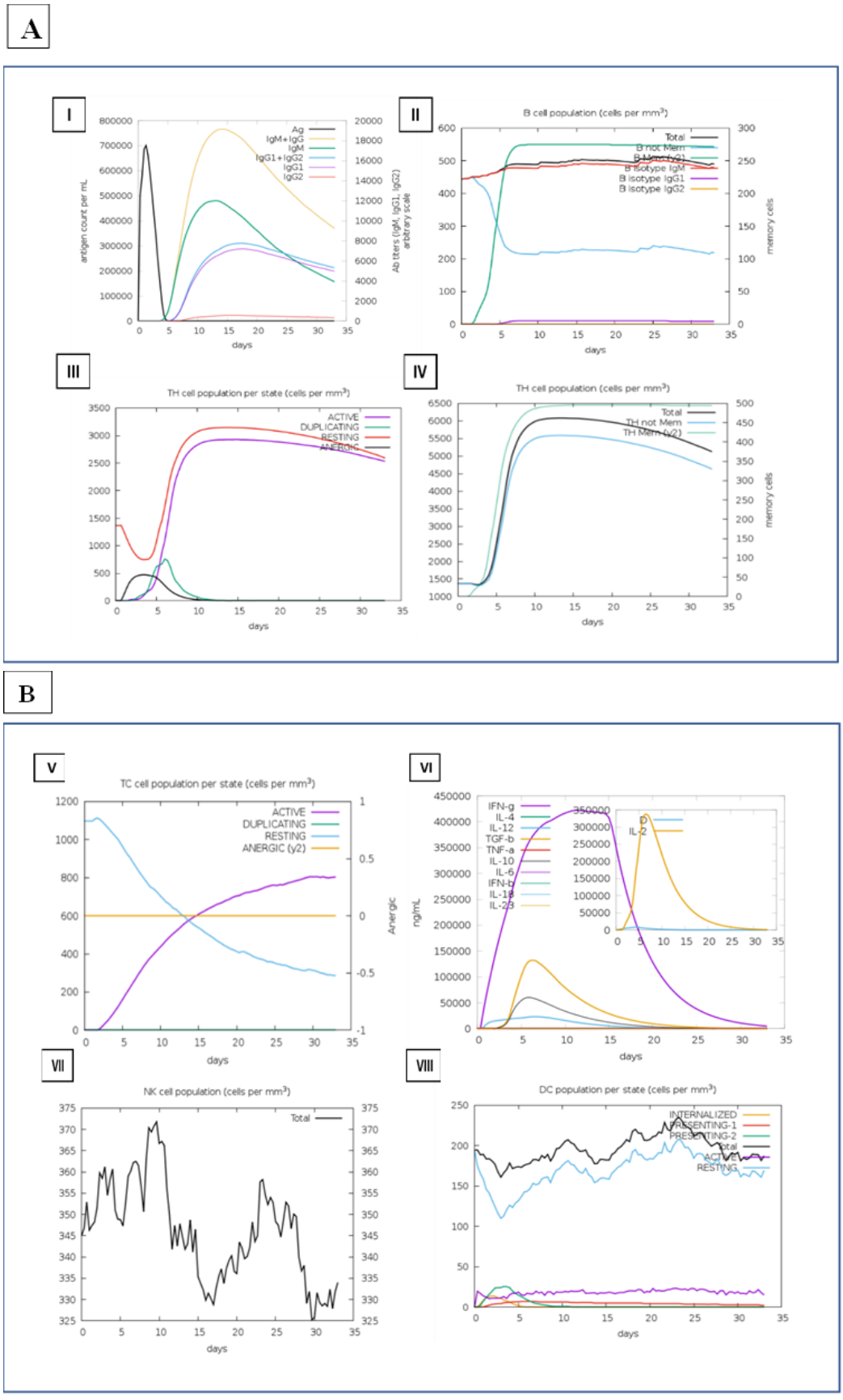

Figure 12. C-ImmSim presentation of an in silico immune simulation with the construct. **A**: (**i**) Production of various types of immunoglobulins, (**ii**) B-cell population, (**iii**) TH cell population per state, (**iv**) T-helper cell population; **B**: (**v**) TC lymphocytes count per entity-state, (**vi**) Different levels of cytokine and interleukins with Simpson index, (**vii**) NK-cell population, (**viii**) Dendritic cell population per state

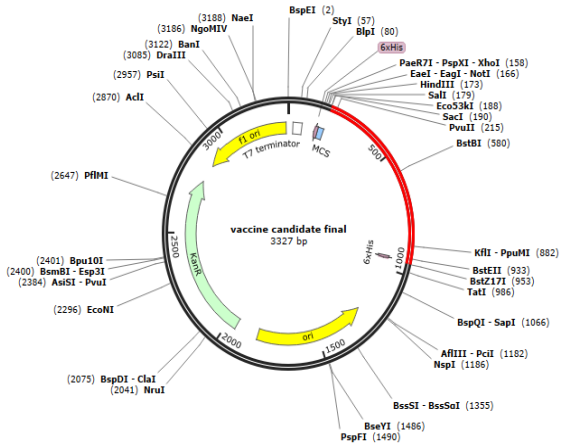

Figure 13. MEV codon-optimized nucleotide sequence for E. coli expression system, in silico cloned at the multiple cloning site (MCS) of the pET28a (+) vector, shown in red color in the vector backbone (black color).

Molecular docking of the 9-mer and 15-mer epitopes with MHC class I and II molecules further supported plausible peptide-MHC interactions [88]. However, docking only indicates predicted binding orientation and structural compatibility; it does not experimentally confirm antigen processing, HLA presentation, or T-cell activation.

B-cell epitopes were predicted using ABCpred and BepiPred and screened for antigenicity, allergenicity, toxicity, hydrophilicity/surface accessibility, and conservancy **(Table 8)**. The top five B-cell epitopes—SGPSTGGNGSFNYSKT (LukS-PVB1), SKSVQWGIKANSFITS (LukS-PVB2), SHEKGSGDTSEFEITY (LukS-PVB3), EVERQNSKSVQWGIKA (LukS-PVB4), and NPSFIATVSHEKGSGD (LukS-PVB5)—were selected based on their predicted antigenicity, non-allergenic nature, non-toxic profile, and high conservation. These B-cell epitopes were included to support humoral immune recognition, while the T-cell epitopes were intended to promote cellular immune responses.

The final multi-epitope vaccine construct was designed with a 50S ribosomal protein L7/L12 adjuvant at the N-terminus to enhance immunogenicity, followed by an EAAAK linker to provide structural rigidity and spatial separation from the epitope region **(Table 9)** [56]. The selected T-cell and B-cell epitopes were joined using GPGPG linkers, which are commonly used to preserve epitope independence and improve antigen processing [57]. A 6×His-tag was added at the C-terminus to facilitate downstream purification. The construct was subsequently evaluated through physicochemical analysis, codon optimization/expression-related prediction, secondary-structure prediction, tertiary-structure modeling, and structural validation. PROCHECK analysis supported the stereochemical quality of the final modeled structure **(Figure 9).**

HDOCK was used to evaluate the interaction between the multi-epitope vaccine construct and Toll-like receptor 2 (TLR2). TLRs are pattern-recognition receptors expressed by innate immune cells such as dendritic cells and macrophages, and contribute to microbial recognition during early immune responses [89]. TLR2 is particularly relevant in *S. aureus* immune recognition because it senses several staphylococcal components, especially lipoproteins and related pathogen-associated molecular patterns [90]. Docking predicted a favorable interaction between the chimeric vaccine construct and TLR2 (Fig. 10), supporting its potential immune receptor compatibility. Toll-like receptor 2 (TLR2) is a crucial pattern-recognition receptor in the innate immune system that enables early detection of Gram-positive bacteria, including *S. aureus*. It identifies conserved microbial components, such as lipoproteins and cell wall-derived molecules, and activates downstream MyD88-dependent signaling, leading to activation of the NF-κB and MAPK pathways. This signaling cascade drives the production of key inflammatory cytokines, which are essential for initiating effective immune responses. In this study, the stable docking interaction observed between the designed LukS-PV multi-epitope vaccine construct and TLR2 suggests strong immunological relevance. Such binding indicates the potential of the construct to effectively engage innate immune signaling pathways, promote dendritic cell activation, and enhance downstream adaptive immune responses. Given the established role of TLR2 in host defense against S. aureus, this interaction further supports the potential immunogenic effectiveness of the proposed vaccine candidate [91,92].

Molecular dynamics simulation further supported the docking result by allowing relaxation of the peptide–receptor complex under dynamic conditions **(Figure 11)**. The maintained interfacial contacts, especially the hydrogen bonds and the salt bridge between arginine at position 31 of chain B and glutamic acid at position 80 of chain A, indicate that the predicted binding interface may remain stable after structural equilibration **(Table 9)**.

Immune simulation showed a theoretical immune response pattern following repeated antigen exposure, including increased memory B-cell and T-cell populations, persistent B-cell memory, and helper T-cell stimulation (**Figure 12**). These results suggest that the construct may induce both humoral and cellular responses. However, immune simulation remains only supportive computational evidence. Experimental validation through HLA-binding assays, PBMC stimulation, cytokine profiling, antibody neutralization, leukocyte cytotoxicity assays, and animal-model studies is required to confirm immunogenicity, safety, and protective efficacy. Finally, *in silico* cloning was performed to assess the theoretical expression feasibility of the designed construct. The vaccine sequence was reverse-translated, codon-optimized according to the selected bacterial host, and virtually inserted into the expression vector **(Figure 13)**. This supports the theoretical feasibility of recombinant expression and downstream purification, although actual expression efficiency, solubility, and yield must be confirmed experimentally.

Several previous studies have investigated PVL or LukS-PV as a vaccine target. Brown et al. reported that LukS-PV immunization protected mice against lung and skin infections caused by *S. aureus* USA300 [93]. A later study identified LukS-PV T-cell-reactive peptide regions, including 149–173, 169–193, and 289–312, with the 169–193 region showing strong proliferative activity [94]. Karauzum et al. developed attenuated LukS-PV and LukF-PV subunit vaccines based on structural modification of the toxin components [95], while Adhikari et al. showed that antibodies against attenuated LukS-PV could neutralize several bicomponent leukotoxin pairs [96]. Recombinant LukS-PV has also been evaluated in healthy adults, and PVL components have been incorporated into multicomponent toxoid vaccine platforms such as IBT-V02 [97,98].

The present study differs from these previous approaches in both antigen design and the logic of epitope selection. Earlier studies mainly used whole/recombinant LukS-PV, attenuated LukS-PV/LukF-PV proteins, or multicomponent toxoid formulations. In contrast, our study used a conserved-region-guided nested T-cell epitope design strategy. First, conserved 9-mer core peptides were identified as predicted MHC class I binders capable of stimulating CD8+ cytotoxic T-cell responses. Each selected 9-mer core was then expanded by six amino acids on both sides to create a 21-mer local sequence context. From this enlarged 21-mer region, a 15-mer peptide was selected, retaining the original 9-mer core in the final sequence. This design allows the 15-mer peptide to be evaluated as a predicted MHC class II binder while preserving the embedded MHC-I-binding 9-mer core. This nested 9-mer/15-mer strategy is important because MHC class I molecules generally present short peptides, often 8–10 amino acids, to CD8+ T cells, whereas MHC class II molecules present longer peptides to CD4+ helper T cells and commonly use a 9-residue binding core within a longer peptide sequence [42,45,99]–[101]. Therefore, a 15-mer peptide containing a conserved 9-mer MHC-I core may theoretically support both cytotoxic and helper T-cell response potential from the same conserved LukS-PV region. To the best of our knowledge, this conserved nested MHC-I/MHC-II epitope design has not previously been reported for LukS-PV-based vaccine development. This represents the main methodological novelty of the present study.

However, the proposed advantage remains computational and requires experimental confirmation. The predicted dual T-cell activity should be validated through HLA-binding assays, antigen-presentation studies, CD8+ and CD4+ T-cell activation assays, cytokine profiling, and in vivo immunogenicity studies. Thus, the present construct should be considered an early-stage immunoinformatics-derived vaccine candidate rather than definitive evidence of protection against MRSA or MSSA infection.

5. LIMITATIONS OF THE STUDY

This study was conducted entirely using immunoinformatics and other *in silico* approaches; therefore, the predicted antigenicity, epitope immunogenicity, receptor binding, molecular dynamics stability, immune simulation, and recombinant expression potential should be interpreted as theoretical findings. Although the designed LukS-PV-based multi-epitope vaccine construct showed favorable computational profiles, these predictions cannot fully capture the complexity of biological systems, including antigen processing, HLA presentation, protein expression, folding, immune cell activation, cytokine responses, and protective efficacy. In addition, molecular docking and molecular dynamics simulation provide useful structural insights but do not replace experimental binding, stability, neutralization, or cytotoxicity assays. Therefore, further laboratory and *in vivo* validation is required before the proposed construct can be considered a confirmed vaccine candidate.

6. CONCLUSION

In conclusion, this study presents a comprehensive immunoinformatics-based framework for the design of a conserved LukS-PV-derived multi-epitope vaccine candidate targeting PVL-positive *S. aureus*, with theoretical applicability to both MRSA and MSSA strains harboring PVL-associated virulence determinants. The selected epitopes demonstrated strong predicted antigenicity, non-allergenicity, non-toxicity, high MHC-binding affinity, broad population coverage, and favorable structural and physicochemical properties, supporting their suitability for vaccine development. The final vaccine construct further exhibited stable immune-receptor interactions, acceptable molecular dynamics behavior, immune simulation profiles, and successful in silico cloning efficiency, collectively indicating its potential to elicit robust humoral and cellular immune responses. Importantly, the construct excludes the intact PVL toxin architecture and the complete LukS-PV/LukF-PV pore-forming system, thereby minimizing any theoretical risk of PVL-like cytolytic activity.

Overall, these findings provide a rational and structurally guided computational strategy for targeting conserved LukS-PV epitopes in PVL-positive *S. aureus*. However, despite these promising in silico outcomes, experimental validation-including recombinant expression, HLA binding assays, PBMC stimulation, cytokine profiling, neutralization studies, cytotoxicity evaluation, and *in vivo* immunization models-remains essential to confirm immunogenicity, safety, and protective efficacy.

Supplementary Materials

The supplementary data supporting the findings of this study are available at Zenodo: https://doi.org/10.5281/zenodo.20951140

Author's ORCID iDs

Prottay Choudhury: https://orcid.org/0009-0003-3165-3186
Md. Saiful Islam: https://orcid.org/0009-0007-4465-489X
Synchita Majumder Kaya: https://orcid.org/0009-0008-8970-4085
Umma Salma Mim: https://orcid.org/0009-0009-0843-1060
Shibashish Sarker: https://orcid.org/0009-0005-6306-7792
K. M. Kaderi Kibria: https://orcid.org/0000-0002-8741-2918

Author Contributions

Conceptualization: KMKK; Methodology: PC, MSI, and SMK; Software: PC; Validation: PC, MSI, and KMKK; Formal Analysis: PC; Investigation: PC, MSI, SMK, USM, and SA; Data Curation: PC; Writing-Original Draft Preparation: PC; Writing-Review and Editing: PC, MSI, SMK, USM, and KMKK; Visualization: PC; Supervision: KMKK; Project Administration: KMKK All authors have read and agreed to the published version of the manuscript.

Funding

This research received no external funding.

Institutional Review Board Statement

Not applicable.

Informed Consent Statement

Not applicable.

Data Availability Statement

The data supporting the findings of this study are available from the corresponding author upon reasonable request.

Acknowledgments

The authors acknowledge the Department of Biotechnology and Genetic Engineering, Mawlana Bhashani Science and Technology University, Tangail, Bangladesh, for providing the academic and research environment that supported this study.

Artificial Intelligence (AI) Declaration

No artificial intelligence (AI) was used in the design, conduct, analysis, interpretation, or preparation of this manuscript.

Conflicts of Interest

The authors declare no conflicts of interest.

References

1. Gould D, Chamberlaine A. *Staphylococcus aureus*: a review of the literature. J Clin Nurs. 1995;4(1), doi:10.1111/j.1365-2702.1995.tb00004.x
2. Tong SY, Davis JS, Eichenberger E, Holland TL, Fowler Jr VG. *Staphylococcus aureus* infections: epidemiology, pathophysiology, clinical manifestations, and management. Clin Microbiol Rev. 2015;28(3):603-61, doi:10.1128/cmr.00134-14
3. Lowy FD. *Staphylococcus aureus* infections. N Engl J Med. 1998;339(8):520-32, doi:10.1056/NEJM199808203390806
4. Guo Y, Song G, Sun M, Wang J, Wang Y. Prevalence and therapies of antibiotic-resistance in *Staphylococcus aureus*. Front Cell Infect Microbiol. 2020;10:107, doi:10.3389/fcimb.2020.00107
5. Wertheim HF, Melles DC, Vos MC, Van Leeuwen W, Van Belkum A, Verbrugh HA, Nouwen JL. The role of nasal carriage in *Staphylococcus aureus* infections. Lancet Infect Dis. 2005;5(12):751-62, doi:10.1016/S1473-3099(05)70295-4
6. Kirby WM. Extraction of a highly potent penicillin inactivator from penicillin resistant staphylococci. Science. 1944;99(2579):452-3, doi:10.1126/science.99.2579.452
7. Turner NA, Sharma-Kuinkel BK, Maskarinec SA, Eichenberger EM, Shah PP, Carugati M, Holland TL, Fowler Jr VG. Methicillin-resistant *Staphylococcus aureus*:

an overview of basic and clinical research. Nat Rev Microbiol. 2019;17(4):203-18, doi:10.1038/s41579-018-0147-4

8. Kalu IC, Kao CM, Fritz SA. Management and prevention of *Staphylococcus aureus* infections in children. Infect Dis Clin North Am. 2022;36(1):73-100, doi:10.1016/j.idc.2021.11.006

9. Nandhini P, Kumar P, Mickymaray S, Alothaim AS, Somasundaram J, Rajan M. Recent developments in methicillin-resistant *Staphylococcus aureus* (MRSA) treatment: a review. Antibiotics. 2022;11(5):606, doi:10.3390/antibiotics11050606

10. Hartman BJ, Tomasz A. Low-affinity penicillin-binding protein associated with beta-lactam resistance in *Staphylococcus aureus*. J Bacteriol. 1984;158(2):513-6, doi:doi.org/10.1128/jb.158.2.513-516.1984

11. Reynolds PE, Brown DF. Penicillin-binding proteins of β-lactam-resistant strains of *Staphylococcus aureus*: effect of growth conditions. FEBS Lett. 1985;192(1):28-32, doi:10.1016/0014-5793(85)80036-3

12. Utsui YU, Yokota TA. Role of an altered penicillin-binding protein in methicillin-and cephem-resistant *Staphylococcus aureus*. Antimicrob Agents Chemother. 1985;28(3):397-403, doi:doi.org/10.1128/aac.28.3.397

13. Matsuhashi MI, Song MD, Ishino FU, Wachi MA, Doi MA, Inoue MA, Ubukata KI, Yamashita NA, Konno MA. Molecular cloning of the gene of a penicillin-binding protein supposed to cause high resistance to beta-lactam antibiotics in *Staphylococcus aureus*. J Bacteriol. 1986;167(3):975-80, doi:10.1128/jb.167.3.975-980.1986

14. Tobin EH, Jogu P, Koirala J. Methicillin-resistant *Staphylococcus aureus*. In StatPearls [internet] 2025. StatPearls Publishing. [cited 2026 June 14]. Available from: https://www.ncbi.nlm.nih.gov/books/NBK482221/

15. Maree M, Thi Nguyen LT, Ohniwa RL, Higashide M, Msadek T, Morikawa K. Natural transformation allows transfer of SCC mec-mediated methicillin resistance in *Staphylococcus aureus* biofilms. Nat Commun. 2022;13(1):2477, doi:10.1038/s41467-022-29877-2

16. Coombs GW, Baines SL, Howden BP, Swenson KM, O'Brien FG. Diversity of bacteriophages encoding Panton-Valentine leukocidin in temporally and geographically related *Staphylococcus aureus*. PLoS One. 2020;15(2):e0228676, doi:10.1371/journal.pone.0228676

17. Darboe S, Dobreniecki S, Jarju S, Jallow M, Mohammed NI, Wathuo M, Ceesay B, Tweed S, Basu Roy R, Okomo U, Kwambana-Adams B. Prevalence of Panton-Valentine leukocidin (PVL) and antimicrobial resistance in community-acquired clinical *Staphylococcus aureus* in an urban Gambian hospital: a 11-year period retrospective pilot study. Front Cell Infect Microbiol. 2019;9:170, doi:10.3389/fcimb.2019.00170

18. Saeed K, Gould I, Esposito S, Ahmad-Saeed N, Ahmed SS, Alp E, Bal AM, Bassetti M, Bonnet E, Chan M, Coombs G. Panton–Valentine leukocidin-positive *Staphylococcus aureus*: a position statement from the International Society of Chemotherapy. Int J Antimicrob Agents. 2018 Jan 1;51(1):16-25, doi:10.1016/j.ijantimicag.2017.11.002

19. Simon SD. Centers for Disease Control and Prevention (CDC). In: Schintler LA, McNeely CL, editors. Encyclopedia of Big Data. Cham: Springer International Publishing; 2022. p. 158-161. doi:10.1007/978-3-319-32001-4_258-1

20. Murray CJ, Ikuta KS, Sharara F, Swetschinski L, Aguilar GR, Gray A, Han C, Bisignano C, Rao P, Wool E, Johnson SC. Global burden of bacterial antimicrobial resistance in 2019: a systematic analysis. Lncet. 2022;399(10325):629-55, doi:10.1016/S0140-6736(21)02724-0

21. Gordon J. Clinical significance of methicillin-sensitive and methicillin-resistant *Staphylococcus aureus* in UK hospitals and the relevance of povidone-iodine in their control. Postgrad Med J. 1993;69:S106-16.

22. Parsons JB, Westgeest AC, Conlon BP, Fowler Jr VG. Persistent methicillin-resistant *Staphylococcus aureus* bacteremia: host, pathogen, and treatment. Antibiotics. 2023;12(3):455, doi:10.3390/antibiotics12030455

23. Klimka A, Mertins S, Nicolai AK, Rummler LM, Higgins PG, Günther SD, Tosetti B, Krut O, Krönke M. Epitope-specific immunity against *Staphylococcus aureus* coproporphyrinogen III oxidase. npj Vaccines. 2021;6(1):11, doi:10.1038/s41541-020-00268-2

24. Zhou P, Shi X, Xia J, Wang Y, Dong S. Innovative epitopes in *Staphylococcal* Protein-A an immuno-informatics approach to combat MDR-MRSA infections. Front Cell Infect Microbiol. 2025;14:1503944, doi:10.3389/fcimb.2024.1503944

25. Tsai CM, Caldera J, Hajam IA, Liu GY. Toward an effective *Staphylococcus* vaccine: why have candidates failed and what is the next step?. Expert Rev Vaccines. 2023;22(1):207-9, doi:10.1080/14760584.2023.2179486

26. Clegg J, Soldaini E, McLoughlin RM, Rittenhouse S, Bagnoli F, Phogat S. *Staphylococcus aureus* vaccine research and development: the past, present and future, including novel therapeutic strategies. Front Immunol. 2021;12:705360., doi:10.3389/fimmu.2021.705360

27. Lina G, Piémont Y, Godail-Gamot F, Bes M, Peter MO, Gauduchon V, Vandenesch F, Etienne J. Involvement of Panton-Valentine leukocidin—producing *Staphylococcus aureus* in primary skin infections and pneumonia. Clin Infect Dis. 1999 Nov 1;29(5):1128-32, doi:10.1086/313461

28. Spaan AN, Vrieling M, Wallet P, Badiou C, Reyes-Robles T, Ohneck EA, Benito Y, De Haas CJ, Day CJ, Jennings MP, Lina G. The staphylococcal toxins γ-haemolysin AB and CB differentially target phagocytes by employing specific chemokine receptors. Nat Commun. 2014;5(1):5438, doi:10.1038/ncomms6438

29. Shallcross LJ, Fragaszy E, Johnson AM, Hayward AC. The role of the Panton-Valentine leucocidin toxin in staphylococcal disease: a systematic review and meta-analysis. Lancet Infect Dis. 2013;13(1):43-54, doi:10.1016/S1473-3099(12)70238-4

30. Spaan AN, Henry T, Van Rooijen WJ, Perret M, Badiou C, Aerts PC, Kemmink J, de Haas CJ, van Kessel KP, Vandenesch F, Lina G. The staphylococcal toxin Panton-Valentine Leukocidin targets human C5a receptors. Cell Host Microbe. 2013;13(5):584-94, doi:10.1016/j.chom.2013.04.006

31. Fowler Jr VG, Proctor RA. Where does a *Staphylococcus aureus* vaccine stand?. Clin Microbiol Infect. 2014;20:66-75, doi:10.1111/1469-0691.12570

32. Rappuoli R, Bottomley MJ, D'Oro U, Finco O, De Gregorio E. Reverse vaccinology 2.0: Human immunology instructs vaccine antigen design. J Exp Med. 2016;213(4):469-81, doi:10.1084/jem.20151960

33. Naz A, Awan FM, Obaid A, Muhammad SA, Paracha RZ, Ahmad J, Ali A. Identification of putative vaccine candidates against Helicobacter pylori exploiting

exoproteome and secretome: a reverse vaccinology based approach. Infect Genet Evol. 2015;32:280-91, doi:10.1016/j.meegid.2015.03.027

34. Flower DR, Macdonald IK, Ramakrishnan K, Davies MN, Doytchinova IA. Computer aided selection of candidate vaccine antigens. Immunome Res. 2010;6(Suppl 2):S1, doi:10.1186/1745-7580-6-S2-S1

35. Jansen KU, Girgenti DQ, Scully IL, Anderson AS. Vaccine review:"Staphyloccocus aureus vaccines: problems and prospects". Vaccine. 2013;31(25):2723-30. doi:10.1016/j.vaccine.2013.04.002

36. Qamar MTU, Ahmad S, Fatima I, Ahmad F, Shahid F, Naz A, Abbasi SW, Khan A, Mirza MU, Ashfaq UA, Chen LL. Designing multi-epitope vaccine against *Staphylococcus aureus* by employing subtractive proteomics, reverse vaccinology and immuno-informatics approaches. Comput Biol Med. 2021;132:104389, doi:10.1016/j.compbiomed.2021.104389

37. Chatterjee R, Sahoo P, Mahapatra SR, Dey J, Ghosh M, Kushwaha GS, Misra N, Suar M, Raina V, Son YO. Development of a conserved chimeric vaccine for induction of strong immune response against *Staphylococcus aureus* using immunoinformatics approaches. Vaccines. 2021;9(9):1038, doi:10.3390/vaccines9091038

38. Wheeler DL, Barrett T, Benson DA, Bryant SH, Canese K, Chetvernin V, Church DM, DiCuccio M, Edgar R, Federhen S, Feolo M. Database resources of the National Center for Biotechnology Information. Nucleic Acids Res. 2007;36(suppl_1):D13-21, doi:10.1093/nar/gkm1000

39. Doytchinova IA, Flower DR. VaxiJen: a server for prediction of protective antigens, tumour antigens and subunit vaccines. BMC Bioinformatics. 2007;8(1):4, doi:10.1186/1471-2105-8-4

40. Yu NY, Wagner JR, Laird MR, Melli G, Rey S, Lo R, Dao P, Sahinalp SC, Ester M, Foster LJ, Brinkman FS. PSORTb 3.0: improved protein subcellular localization prediction with refined localization subcategories and predictive capabilities for all prokaryotes. Bioinformatics. 2010 Jul 1;26(13):1608-15, doi:10.1093/bioinformatics/btq249

41. Buus S, Lauemøller SL, Worning P, Kesmir C, Frimurer T, Corbet S, Fomsgaard A, Hilden J, Holm A, Brunak S. Sensitive quantitative predictions of peptide-MHC binding by a 'Query by Committee'artificial neural network approach. Tissue Antigens. 2003;62(5):378-84, doi:10.1034/j.1399-0039.2003.00112.x

42. Wang P, Sidney J, Dow C, Mothé B, Sette A, Peters B. A systematic assessment of MHC class II peptide binding predictions and evaluation of a consensus approach. PLoS Comput Biol. 2008;4(4):e1000048, doi:10.1371/journal.pcbi.1000048

43. Wang P, Sidney J, Kim Y, Sette A, Lund O, Nielsen M, Peters B. Peptide binding predictions for HLA DR, DP and DQ molecules. BMC Bioinformatics. 2010;11(1):568, doi:10.1186/1471-2105-11-568

44. Peters B, Sette A. Generating quantitative models describing the sequence specificity of biological processes with the stabilized matrix method. BMC Bioinformatics. 2005;6(1):132, doi:10.1186/1471-2105-6-132

45. Munia M, Mahmud S, Mohasin M, Kibria KK. In silico design of an epitope-based vaccine against choline binding protein A of *Streptococcus pneumoniae*. Inform Med Unlocked. 2021;23:100546, doi:10.1016/j.imu.2021.100546

46. Bui HH, Sidney J, Li W, Fusseder N, Sette A. Development of an epitope conservancy analysis tool to facilitate the design of epitope-based diagnostics and vaccines. BMC Bioinformatics. 2007;8(1):361, doi:10.1186/1471-2105-8-361

47. Dimitrov I, Bangov I, Flower DR, Doytchinova I. AllerTOP v. 2—a server for in silico prediction of allergens. J Mol Model. 2014;20(6):2278, doi:10.1007/s00894-014-2278-5

48. Gupta S, Kapoor P, Chaudhary K, Gautam A, Kumar R, Open Source Drug Discovery Consortium, Raghava GP. In silico approach for predicting toxicity of peptides and proteins. PLoS One. 2013;8(9):e73957, doi:10.1371/journal.pone.0073957

49. Chen Y, Yu P, Luo J, Jiang Y. Secreted protein prediction system combining CJ-SPHMM, TMHMM, and PSORT. Mamm Genome. 2003;14(12):859-65., doi:10.1007/s00335-003-2296-6

50. Berman HM, Westbrook J, Feng Z, Gilliland G, Bhat TN, Weissig H, Shindyalov IN, Bourne PE. The protein data bank. Nucleic Acids Res. 2000;28(1):235-42, doi:10.1093/nar/28.1.235

51. Wang Q, He J, Wu D, Wang J, Yan J, Li H. Interaction of α-cyperone with human serum albumin: Determination of the binding site by using Discovery Studio and via spectroscopic methods. J Lumin. 2015;164:81-5, doi:10.1016/j.jlumin.2015.03.025

52. Nair DT, Singh K, Siddiqui Z, Nayak BP, Rao KV, Salunke DM. Epitope recognition by diverse antibodies suggests conformational convergence in an antibody response. The J Immunol. 2002;168(5):2371-82, doi:10.4049/jimmunol.168.5.2371

53. Saha S, Raghava GP. Prediction of continuous B-cell epitopes in an antigen using recurrent neural network. Proteins. 2006;65(1):40-8, doi:10.1002/prot.21078

54. Jespersen MC, Peters B, Nielsen M, Marcatili P. BepiPred-2.0: improving sequence-based B-cell epitope prediction using conformational epitopes. Nucleic Acids Res. 2017;45(W1):W24-9, doi:10.1093/nar/gkx346

55. Akter A, Ananna NF, Ullah H, Islam S, Al Amin M, Kibria KK, Mahmud S. Computational approach for identifying immunogenic epitopes and optimizing peptide vaccine through in-silico cloning against Mycoplasma genitalium. Heliyon. 2024;10(7), doi:10.1016/j.heliyon.2024.e28223

56. adilah F, Paramita RI, Erlina L, Istiadi KA, Wuyung PE, Tedjo A. Linker optimization in breast cancer multiepitope peptide vaccine design based on molecular study. In: Proceedings of the 4th International Conference on Life Sciences and Biotechnology (ICOLIB 2021); 2022; Atlantis Press. p. 528-538. doi:10.2991/978-94-6463-062-6.

57. Yousaf H, Naz A. Exploring B and T-cell epitopes for constructing a Novel Multiepitope vaccine to combat emerging Monkeypox infection: A Reverse Vaccinology approach. bioRxiv. 2022:2022-12, doi:10.1101/2022.12.09.519581

58. Ayyagari VS, TC V, K AP, Srirama K. Design of a multi-epitope-based vaccine targeting M-protein of SARS-CoV2: an immunoinformatics approach. J Biomol Struct Dyn. 2022;40(7):2963-77, doi:10.1080/07391102.2020.1850357

59. Hebditch M, Carballo-Amador MA, Charonis S, Curtis R, Warwicker J. Protein–Sol: a web tool for predicting protein solubility from sequence. Bioinformatics.

2017;33(19):3098-100, doi:10.1093/bioinformatics/btx345

60. McGuffin LJ, Bryson K, Jones DT. The PSIPRED protein structure prediction server. Bioinformatics. 2000;16(4):404-5, doi:10.1093/bioinformatics/16.4.404

61. Du Z, Su H, Wang W, Ye L, Wei H, Peng Z, Anishchenko I, Baker D, Yang J. The trRosetta server for fast and accurate protein structure prediction. Na Protoc. 2021;16(12):5634-51, doi:10.1038/s41596-021-00628-9

62. Laskowski RA, Rullmann JA, MacArthur MW, Kaptein R, Thornton JM. AQUA and PROCHECK-NMR: programs for checking the quality of protein structures solved by NMR. J Biomol NMR. 1996;8(4):477-86, doi:10.1007/BF00228148

63. Yan Y, Tao H, He J, Huang SY. The HDOCK server for integrated protein–protein docking. Nat Protoc. 2020;15(5):1829-52, doi:10.1093/nar/gkx407

64. Maestro S. Maestro. Schrödinger, LLC, New York, NY. 2020;2020:682.

65. Rapin N, Lund O, Bernaschi M, Castiglione F. Computational immunology meets bioinformatics: the use of prediction tools for molecular binding in the simulation of the immune system. PLoS One. 2010;5(4):e9862, doi:10.1371/journal.pone.0009862

66. Tahir ul Qamar M, Rehman A, Tusleem K, Ashfaq UA, Qasim M, Zhu X, Fatima I, Shahid F, Chen LL. Designing of a next generation multiepitope based vaccine (MEV) against SARS-COV-2: Immunoinformatics and in silico approaches. PLoS One. 2020;15(12):e0244176, doi:10.1371/journal.pone.0244176

67. Chauhan V, Singh MP. Immuno-informatics approach to design a multi-epitope vaccine to combat cytomegalovirus infection. Eur J Pharm Sci. 2020;147:105279, doi:10.1016/j.ejps.2020.105279

68. Kroger AT, Sumaya CV, Pickering LK, Atkinson WL. General recommendations on immunization. MMWR Recomm Rep. 2011;60(2):1-64.

69. Castiglione F, Mantile F, De Berardinis P, Prisco A. How the interval between prime and boost injection affects the immune response in a computational model of the immune system. Comput Math Methods Med. 2012;2012(1):842329, doi:10.1155/2012/842329

70. Nain Z, Abdulla F, Rahman MM, Karim MM, Khan MS, Sayed SB, Mahmud S, Rahman SR, Sheam MM, Haque Z, Adhikari UK. Proteome-wide screening for designing a multi-epitope vaccine against emerging pathogen Elizabethkingia anophelis using immunoinformatic approaches. J Biomol Struct Dyn. 2020;38(16):4850-67, doi:10.1080/07391102.2019.1692072

71. Grote A, Hiller K, Scheer M, Münch R, Nörtemann B, Hempel DC, Jahn D. JCat: a novel tool to adapt codon usage of a target gene to its potential expression host. Nucleic Acids Res. 2005;33(suppl_2):W526-31, doi:10.1093/nar/gki376

72. Smith CL, Econome JG, Schutt A, Klco S, Cantor CR. A physical map of the Escherichia coli K12 genome. Science. 1987;236(4807):1448-53, doi:10.1126/science.329619

73. Sharp PM, Li WH. The codon adaptation index-a measure of directional synonymous codon usage bias, and its potential applications. Nucleic Acids Res. 1987;15(3):1281-95, doi:10.1093/nar/15.3.1281

74. Fowler VG, Allen KB, Moreira ED, Moustafa M, Isgro F, Boucher HW, Corey GR, Carmeli Y, Betts R, Hartzel JS, Chan IS. Effect of an investigational vaccine for preventing *Staphylococcus aureus* infections after cardiothoracic surgery: a randomized trial. JAMA. 2013;309(13):1368-78, doi:10.1001/jama.2013.3010

75. Harro CD, Betts RF, Hartzel JS, Onorato MT, Lipka J, Smugar SS, Kartsonis NA. The immunogenicity and safety of different formulations of a novel *Staphylococcus aureus* vaccine (V710): results of two Phase I studies. Vaccine. 2012;30(9):1729-36, doi:10.1016/j.vaccine.2011.12.045

76. Grebe T, Sarkari MT, Cherkaoui A, Schaumburg F. Exploration of compounds to inhibit the Panton-Valentine leukocidin of *Staphylococcus aureus*. Med Microbiol Immunol. 2024;213(1):19, doi:10.1007/s00430-024-00803-1

77. Tristan A, Benito Y, Montserret R, Boisset S, Dusserre E, Penin F, Ruggiero F, Etienne J, Lortat-Jacob H, Lina G, Bowden MG. The signal peptide of *Staphylococcus aureus* panton valentine leukocidin LukS component mediates increased adhesion to heparan sulfates. PLoS One. 2009;4(4):e5042, doi:10.1371/journal.pone.0005042

78. Müller E, Monecke S, Armengol Porta M, Narvaez Encalada MV, Reissig A, Rüttiger L, Schröttner P, Schwede I, Söffing HH, Thürmer A, Ehricht R. Rapid Detection of Panton–Valentine Leukocidin Production in Clinical Isolates of *Staphylococcus aureus* from Saxony and Brandenburg and Their Molecular Characterisation. Pathogens. 2025;14(3):238, doi:10.3390/pathogens14030238

79. Garbo V, Venuti L, Boncori G, Albano C, Condemi A, Natoli G, Frasca Polara V, Billone S, Canduscio LA, Cascio A, Colomba C. Severe Panton–Valentine-Leukocidin-Positive Staphylococcus Aureus Infections in Pediatric Age: A Case Report and a Literature Review. Antibiotics. 2024;13(12):1192, doi:10.3390/antibiotics13121192

80. Foster TJ. Immune evasion by staphylococci. Nat Rev Microbiol. 2005;3(12):948-58, doi:10.1038/nrmicro3521

81. Otto M. Basis of virulence in community-associated methicillin-resistant *Staphylococcus aureus*. Annu Rev Microbiol. 2010;64:143-62, doi:10.1146/annurev.micro.112408.134309

82. Lina G, Piémont Y, Godail-Gamot F, Bes M, Peter MO, Gauduchon V, Vandenesch F, Etienne J. Involvement of Panton-Valentine leukocidin—producing *Staphylococcus aureus* in primary skin infections and pneumonia. Clin Infect Dis. 1999;29(5):1128-32, doi:10.1086/313461

83. Tromp AT, Van Strijp JA. Studying staphylococcal leukocidins: a challenging endeavor. Front Microbiol. 2020;11:611, doi:10.3389/fmicb.2020.00611

84. Arnon R, Ben-Yedidia T. Old and new vaccine approaches. Int Immunopharmacol. 2003;3(8):1195-204, doi:10.1016/S1567-5769(03)00016-X

85. Negahdaripour M, Nezafat N, Eslami M, Ghoshoon MB, Shoolian E, Najafipour S, Morowvat MH, Dehshahri A, Erfani N, Ghasemi Y. Structural vaccinology considerations for in silico designing of a multi-epitope vaccine. Infect Genet Evol. 2018;58:96-109, doi:10.1016/j.meegid.2017.12.008

86. De Groot AS, Moise L, McMurry JA, Martin W. Epitope-based immunome-derived vaccines: a strategy for improved design and safety. In: Falus A, editor. Clinical Applications of Immunomics. Immunomics Reviews. Vol. 2. New York (NY): Springer; 2008. p. 39–69. doi:10.1007/978-0-387-79208-8_3

87. Skwarczynski M, Toth I. Peptide-based synthetic vaccines.

Chem Sci. 2016;7(2):842-54, doi:10.1039/C5SC03892H

88. Michel-Todó L, Reche PA, Bigey P, Pinazo MJ, Gascón J, Alonso-Padilla J. In silico design of an epitope-based vaccine ensemble for Chagas disease. Front Immunol. 2019;10:2698, doi:10.3389/fimmu.2019.02698

89. Kawasaki T, Kawai T. Toll-like receptor signaling pathways. Front Immunol. 2014;5:112681, doi:10.3389/fimmu.2014.00461

90. Fournier B. The function of TLR2 during staphylococcal diseases. Front Cell Infect Microbiol. 2013;2:167, doi:10.3389/fcimb.2012.00167

91. Fournier B, Philpott DJ. Recognition of *Staphylococcus aureus* by the innate immune system. Clin Microbiol Rev. 2005;18(3):521-40, doi:10.1128/cmr.18.3.521-540.2005

92. Yimin, Kohanawa M, Zhao S, Ozaki M, Haga S, Nan G, Kuge Y, Tamaki N. Contribution of toll-like receptor 2 to the innate response against *Staphylococcus aureus* infection in mice. PLoS One. 2013;8(9):e74287, doi:10.1371/journal.pone.0074287

93. Brown EL, Dumitrescu O, Thomas D, Badiou C, Koers EM, Choudhury P, Vazquez V, Etienne J, Lina G, Vandenesch F, Bowden MG. The Panton–Valentine leukocidin vaccine protects mice against lung and skin infections caused by *Staphylococcus aureus* USA300. Clin Microbiol Infect. 2009;15(2):156-64, doi:10.1111/j.1469-0691.2008.02648.x

94. Brown EL, Smith KC, Bowden MG. Identification of a T-cell epitope in the *Staphylococcus aureus* Panton-Valentine LukS-PV component. Open J Immunol. 2012;2(3):111, doi:10.4236/oji.2012.23013

95. Karauzum H, Adhikari RP, Sarwar J, Devi VS, Abaandou L, Haudenschild C, Mahmoudieh M, Boroun AR, Vu H, Nguyen T, Warfield KL. Structurally designed attenuated subunit vaccines for S. aureus LukS-PV and LukF-PV confer protection in a mouse bacteremia model. PLoS One. 2013;8(6):e65384, doi:10.1371/journal.pone.0065384

96. Adhikari RP, Kort T, Shulenin S, Kanipakala T, Ganjbaksh N, Roghmann MC, Holtsberg FW, Aman MJ. Antibodies to S. aureus LukS-PV attenuated subunit vaccine neutralize a broad spectrum of canonical and non-canonical bicomponent leukotoxin pairs. PLoS One. 2015;10(9):e0137874, doi:10.1371/journal.pone.0137874

97. Landrum ML, Lalani T, Niknian M, Maguire JD, Hospenthal DR, Fattom A, Taylor K, Fraser J, Wilkins K, Ellis MW, Kessler PD. Safety and immunogenicity of a recombinant *Staphylococcus aureus* α-toxoid and a recombinant Panton-Valentine leukocidin subunit, in healthy adults. Hum Vaccin Immunother. 2017 Apr 3;13(4):791-801, doi:10.1080/21645515.2016.1248326

98. Karauzum H, Venkatasubramaniam A, Adhikari RP, Kort T, Holtsberg FW, Mukherjee I, Mednikov M, Ortines R, Nguyen NT, Doan TM, Diep BA. IBT-V02: A multicomponent toxoid vaccine protects against primary and secondary skin infections caused by *Staphylococcus aureus*. Front Immunol. 2021;12:624310, doi:10.3389/fimmu.2021.624310

99. Nielsen M, Andreatta M, Peters B, Buus S. Immunoinformatics: predicting peptide-MHC binding. Annu Rev Biomed Data Sci. 2020;3:191-215. doi:10.1146/annurev-biodatasci-021920-100259

100. Holland CJ, Cole DK, Godkin A. Redirecting CD4+ T cell responses with the flanking residues of MHC class II-bound peptides: the core is not enough. Front Immunol. 2013;4:172, doi:10.3389/fimmu.2013.00172

101. Laimer J, Lackner P. MHCII3D—Robust structure based prediction of MHC II binding peptides. Int J Mol Sci. 2020;22(1):12, doi:10.3390/ijms22010012